General Disclaimer

One or more of the Following Statements may affect this Document

- This document has been reproduced from the best copy furnished by the organizational source. It is being released in the interest of making available as much information as possible.

- This document may contain data, which exceeds the sheet parameters. It was furnished in this condition by the organizational source and is the best copy available.

- This document may contain tone-on-tone or color graphs, charts and/or pictures, which have been reproduced in black and white.

- This document is paginated as submitted by the original source.

- Portions of this document are not fully legible due to the historical nature of some of the material. However, it is the best reproduction available from the original submission.

STUDIES OF SILICON PN JUNCTION SOLAR CELLS

By

Fredrik A. Lindholm and Arnost Neugroschel
Principal Investigators
Department of Electrical Engineering
University of Florida
Gainesville, Florida 32611

FINAL TECHNICAL REPORT TR No. 77-1
covering the year ending September 1977

prepared for

National Aeronautics and Space Administration
NASA Lewis Research Center
NASA grant NSG-3018

FOREWORD

This report summarizes the major technical findings made in the research program at the University of Florida sponsored by NASA Lewis Research Center under Grant No. NSG-3018. This grant is a continuation of the support began under the same grant number on June 24, 1974. We report here our findings during the year ending September 1977.

The work to be reported came from the efforts of several key people. C.T. Sah suggested to NASA the possibility of placing this grant research at the University of Florida, and afterwards, together with the author, helped make the arrangements and formulate the technical plan of the research. Dr. Sah has contributed significantly to nearly every aspect of the research described in this report. After joining the faculty of the University of Florida in September, 1976, Arnost Neugroschel became a key contributor to the research program. The technical collaboration of M.P. Godlewski and H.W. Brandhorst, Jr., of NASA Lewis Research Center greatly aided the completion of several phases of the research. During the tenure of the NASA grant, the Energy Research and Development Administration began supporting a separate but related research program at the University of Florida under the author's direction. This support aided the research reported here, and made possible a valuable and continuing technical interaction with J.G. Fossum of Sandia Laboratories (ERDA), Albuquerque, New Mexico. In addition to these senior investigators, two graduate students at the University of Florida participated in the research: P.J. Chen and S.C. Pao.

CHAPTER 1 INTRODUCTION

As Brandhorst first noted, the power conversion efficiency of p-substrate, p-n junction silicon solar cells is limited because V_{OC} falls short of theoretical expectations by about 15 percent [1]. Thus, increasing V_{OC} is important in raising efficiency, doubly so because the fill factor FF increases with increasing V_{OC} [2]. Indeed, as we have recently pointed out [3], essentially in agreement with the earlier projection of Brandhorst [1], if V_{OC} were increased to 700 mV, AMO efficiencies in the range of 18 to 20 percent become possible.

1.1 Studies of Basic Mechanisms

Our previous work at Florida under NASA LeRC grant support has proposed methods, based on experiment [4], for determining which of the many fundamental mechanisms [5,6] that can occur in silicon devices are responsible for this discrepancy in V_{OC} in any given solar cell. This work has demonstrated experimentally the important conclusion that the discrepancy originates in the excessive recombination current occurring in the degenerately doped emitter of the cell. In particular, for cells having a base resistivity of about 0.1 Ohm-cm, we demonstrated that the dark recombination current from the quasineutral emitter region exceeded that from the quasineutral base region by more than an order of magnitude [4]. We demonstrated further that both of these recombination currents exceeded the dark recombination current coming from the junction space-charge region. In these demonstrations, the dark cell was biased in the forward direction with a voltage V near 600 mV, which is approximately the value of V_{OC} produced in these cells. The conclusion implied by these experiments is that the large recombination current occurring

either in the bulk of the degenerately doped emitter or at its surface limits V_{OC} and efficiency well below the projections of classical p-n junction theory [1]. This conclusion, based on experiment, contrasts with the recent theoretical suggestions of other authors that field-induced bandgap narrowing in the junction space-charge region is the dominant contributor to the observed performance, including V_{OC} and efficiency, of p-substrate, diffused p-n junction silicon solar cells [7,8].

As yet, the physical mechanisms causing the anomalously large emitter recombination current have not been identified. However, considerable progress has recently been made. Our work at Florida has shown experimentally [9] the decided superiority of forward-biased admittance measurements over open-circuit-voltage-decay (OCVD) measurements in determining the dominant relaxation time [4], originally called the dominant natural mode [10], of the cell. The accurate determination of the dominant relaxation time is crucial to the determination of the minority-carrier charge stored in the quasi-neutral emitter and of the phenomenological carrier lifetime of the emitter, and thus to the determination of the physical mechanisms responsible for the excess emitter recombination current [4]. Furthermore, we have just reported a new method, based on the temperature dependence of the emitter recombination current [11], for determining the bandgap narrowing in the quasi-neutral emitter region as a function of the emitter doping concentration. Bandgap narrowing is believed to be one of the main physical mechanisms that contribute to the discrepancy in V_{OC} [4,5,6]. This new experimental method developed at Florida, together with work just described by Lanyon and co-workers [12] and by Mertens and co-workers [13], may yield insight needed

to better define the fundamental physical mechanisms underlying the V_{OC} discrepancy.

1.2 Studies of HLE Structures for Increasing V_{OC}

In the past year, although our work on fundamental physical mechanisms has continued to some degree, the main attention of the NASA LeRC sponsored research at Florida has shifted toward the demonstration that new device structures can substantially diminish the effects of whatever mechanisms in the emitter may be degrading V_{OC}, without requiring a detailed identification of these mechanisms. This new emphasis led to our proposal, from a theoretical standpoint [14,15], of the high-low-junction emitter (HLE) solar cell, in which the emitter region contains a high-low (H-L) junction. We have demonstrated experimentally [3,16] that this H-L junction can suppress the dark emitter recombination current to levels so low that the emitter current no longer presents an obstable to the achievement of an open-circuit voltage of 700 mV. For test cells we have fabricated at Florida, the open-circuit voltage observed has been mainly determined by the dark base recombination current. Our experiments have shown that large values of V_{OC} result in these HLE test cells, but that values approaching the theoretical limit of 700 mV will require improving the diffusion length of electrons in the quasineutral base region.

The maximum V_{OC} seen to the present has been 640 mV for AM0 illumination. This voltage, which compares with the 600 mV maximum normally seen in p-n junction silicon solar cells, has been measured on an oxide-charge-induced (OCI) HLE structure. In this structure, the H-L junction is formed in emitter material of non-degenerate doping concentration by an oxide-charge-induced electron accumulation layer [3,16]. Open-circuit voltages about 10 mV less have been observed in another type of HLE solar

cell, the diffused-HLE structure, in which impurity diffusion forms the H-L junction in the emitter region.

1.3 Structure of This Report

This report consists of three parts. In the first part, which is Chapter 2, we develop, from a theoretical standpoint, the modifications of the basic Shockley equations that result from the random and non-random spatial variation of the chemical composition of a semiconductor. These modifications underlie the existence of the excessive emitter recombination current that limits the V_{OC} of solar cells. The discussion includes a more rigorous treatment of quasi-fields than has appeared before. In the second part, work related to the measurement of parameters is presented. Chapter 3 treats the measurement of series resistance. Chapter 4 deals with the measurement of the base diffusion length and presents two methods for establishing the energy bandgap narrowing in the heavily-doped emitter region. The discussion in Chapter 5 relates to corrections that can be important in the application of one of these methods to small test cells. In the third part, we briefly describe OCI-HLE test cells which exhibit a considerably higher V_{OC} than was previously seen in n-on-p solar cells.

Insofar as is possible, each of the Chapters are written as independent units to enable the reader with a main interest in a later chapter to be able to read that one directly without first having to become familiar with the earlier chapters.

REFERENCES FOR CHAPTER I

1. H.W. Brandhorst, Jr., Record of 9th Photovoltaic Specialists Conf., 1 (1972).

2. M.A. Green, Solid-State Electron., 20, 265 (1977).

3. F.A. Lindholm, J.G. Fossum, A. Neugroschel, and C.T. Sah, 13th Photovoltaic Specialists Conf., June 1978.

4. F.A. Lindholm, A. Neugroschel, C.T. Sah, M.P. Godlewski, and H.W. Brandhorst, Jr., IEEE Trans. Electron Devices, ED-24, 402 (1977).

5. F.A. Lindholm and C.T. Sah, IEEE Trans. Electron Devices, ED-24, 299 (1977).

6. C.T. Sah and F.A. Lindholm, IEEE Trans. Electron Devices, ED-24, 358 (1977).

7. E.S. Rittner, Tech. Dig. 1976 Int. Electron Devices Meeting, 69 (1976).

8. E.S. Rittner, J. Energy, 1, 9 (1977).

9. A. Neugroschel, P.J. Chen, S.C. Pao, F.A. Lindholm, IEEE Trans. Electron Devices, ED-25, 485 (1978).

10. F.A. Lindholm and C.T. Sah, J. Appl. Phys., 47, 4203 (1976).

11. A. Neugroschel, P.J. Chen, S.C. Pao, and F.A. Lindholm, 13th Photovoltaic Specialists Conf., June 1978.

12. H.P.D. Lanyon, A.K. McCurdy, and R.A. Tuft, 13th IEEE Photovoltaic Spec. Conf., June 1978.

13. J. Van Meerbergen, J. Nijs, R. Mertens, and R. Van Overstraeten, 13th IEEE Photovoltaic Spec. Conf., June 1978.

14. C.T. Sah, F.A. Lindholm, and J.G. Fossum, IEEE Trans. Electron Devices, ED-25, 66 (1978).

15. J.G. Fossum, F.A. Lindholm, and C.T. Sah, 1977 Int. Electron Devices Meeting, 222 (1977).

16. A. Neugroschel, F.A. Lindholm, S.C. Pao, and J.G. Fossum, Appl. Phys. Lett., 168, 15 July 1978.

PART I BASIC MECHANISMS DEGRADING V_{OC}: THEORY

CHAP. 2 CARRIER GENERATION, RECOMBINATION, TRAPPING AND TRANSPORT IN SEMICONDUCTORS WITH POSITION DEPENDENT COMPOSITION

2.1 Introduction

Semiconductor structures and materials with position dependent chemical composition have been of central interest in device applications. For structures with abrupt changes in but otherwise uniform chemical compositions, such as the hetrojunction interfaces of a Schottky barrier or a MOS capacitance, the mathematical analyses of carrier generation, recombination, trapping and transport (GRTT) are based on ideal and position independent energy band models for each material region [1,2]. The solutions of the device characteristics are then obtained by matching the solutions of each of these uniform regions at their interfaces. These solutions are obtained from the following Shockley equations which were first used to get the characteristics of p-n junction diodes and transistors [3,4]. These were generalized to include the most important generation, recombination, trapping and tunneling mechanisms [5] and high-frequency effect [6] near thermal equilibrium as well as hot carrier effects on transport [7].

$$\vec{J}_N = +qD_n \nabla N + q\mu_n N\vec{E} \tag{1}$$

$$= - q\mu_n N \nabla V_N \tag{1a}$$

$$\vec{J}_P = - qD_p \nabla P + q\mu_p P\vec{E} \tag{2}$$

$$= - q\mu_p P \nabla V_P \tag{2a}$$

$$0 = + \nabla \cdot J_N + I_{SS} \tag{3}$$

$$0 = - \nabla \cdot \vec{J}_P + I_{SS} \tag{4}$$

$$\nabla \cdot \vec{E} = - \nabla^2 V_I = \rho/\varepsilon = (q/\varepsilon)(P - N + N_{DD} - N_{AA} - N_T) \tag{5}$$

Here, the coefficients which characterize the material properties and the variables have the usual meaning [5].

When the chemical composition of the material or device structure varies continuously and strongly in a regular or random fashion, the Shockley equations need to be modified. A number of fairly distinct situations can be treated and discussed below.

(1) If the composition varies on an atomic scale but the atomic perturbations are widely separated (concentration less than about 10^{17} perturbations/cm^3), we have the classical case which is contained in the Shockley equations: the mobilities, μ_n and μ_p, the diffusivities, D_n and D_p, and the generation-recombination-trapping rates all vary with position. These material parameters are macroscopic averages taken in regions of sufficiently large volumes to contain many (~10^6) particles (electrons, holes and atoms) to make the statistical fluctuation small.

(2) If the composition variations are on a macroscopic scale (concentrations of the foreign atomic species or physical defects are greater than about 10^{17}cm^{-3} but smaller than about 1% of the host atomic density), the Shockley equations are still applicable. However, the ideal energy band model of allowed band of nonlocalized energy (Bloch) states or levels with sharp band edges separated by forbidden energy gaps must be modified. The modification comes about from the high concentrations of the spatially random atomic perturbations which shift

the band states of the ideal model into the energy gaps, thereby producing a distribution of semi-localized energy gap states both in energy and in position. The deep gap states, which are located far away (many kT/q in energy) from the ideal band edge positions, are nearly true bound states with negligible carrier mobility. They can be accurately included in the generation-recombination-trapping terms of the Shockley equations. However, the shallow gap states, which are located in energy near the ideal band edges, may have appreciable mobility due to the large spatial overlaps of the very extended wave functions. These edge states will modify the macroscopic and thermal averages of the mobilities and diffusivities in the Shockley equations, giving them position, temperature and electric field dependences significantly different from those of the ideal energy band model discussed in case (1). Here, the ideal or sharp band edges lose their significance. To put the physics of this situation into a simple persepctive, Cohen [8] introduced the concept of mobility edge to separate the semi-delocalized edge states from the nearly localized tail states. The modifications of the macroscopic and thermal averages of the mobility and diffusivity from the ideal case, then, come in two factors: the integration limit is now the position of the mobility edge instead of the ideal band edge and the density of state in the integrand is decreased due to the splitting of the band states into the gap. Van Overstraeten [9] has provided an analysis of the mobility in this situation. Although he included the tail states in the mobility and diffusivity averages by assuming that they have the same carrier scattering power or relaxation time as the band states, the errors in computing the diffusion and drift current are probably small since the densities of the electrons or holes trapped at these localized gap states are much smaller than those in the edge and band states.

The effects of the distributed gap states on the carrier generation-recombination rates are well known. It was demonstrated as the principal source of excess current in tunnel diodes [10]. However, a demonstration of the application of this model for calculating the recombination rates is not available. An example will be given in the next section.

(3) If the composition variations are on a chemical scale and continuous over an extended region, basic modifications of the Shockley equations must be made. These modifications can be analyzed by separating out the random and the nonrandom components of the atomic potentials. The random component will produce the modifications to the Shockley equations similar to those discussed in cases (1) and (2). The nonrandom and continuously varying component will produce a corresponding spatial variation of energy levels of the band or Bloch states as well as the semi-localized gap (edge and tail) states. This produces major modifications of the Shockley equation, giving rise to new terms. The position dependent energy level was first analyzed by Kroemer [11] for device applications in graded or position-dependent band gap materials. He began with the effective mass equation and introduced the concept of quasi-electrical fields for electrons and holes.

Although the graded band gap materials have seen little application in conventional transistor devices in the past, it shows promise for improved efficiency in solar cells. Thus, an extension of the Shockley equation for this case will also be presented.

In the next two sections, we shall obtain quantitative results for the generation-recombination rates in the distributed gap states of case (2) and modifications of the Shockley equations in the graded band gap materials of case (3).

2.2 Generation-Recombination-Trapping in Distributed Gap States

For this case, the basic property of the gap states is that each imperfection center, whether having a point, pair or more complex geometry, is separated from its neighboring centers by a distance large compared with extent of the bound state wave function localized at the center. Thus, the transition rate of an electron (or hole) bound to one center to the adjacent centers is much smaller than the rate to the conduction or valence band and edge states. Then, the capture (or emission) rates of electrons (or holes) at each gap-state center can be added to give the total rate.

The above property of independent or noninteracting gap-state centers make the arithematics of the original Shockley-Read derivation [12] of the recombination kinetics directly applicable. If the centers were interacting, then additional rate equations for the bound-to-bound transitions between the centers or between states on one center must be included. This was done previously [5].

For the independent centers, the four electron and hole capture and emission rates between a band state and trap state located at E_T are shown in Figure 1. The transition rates, averaged over the distribution in the conduction or valence band states are just those given by Shockley and Read:

$$a_T = c_n(E_T)n[1-f_T(E_T)]\rho_T(E_T)dE_T \tag{6}$$

$$b_T = e_n(E_T)f_T(E_T)\rho_T(E_T)dE_T \tag{7}$$

$$c_T = c_p(E_T)pf_T(E_T)\rho_T(E_T)dE_T \tag{8}$$

$$d_T = e_p(E_T)[1-f_T(E_T)]\rho_T(E_T)dE_T \tag{9}$$

In Equation (6), c_n is the macroscopic averaged capture probability rate ($\#/cm^3$-sec) of electrons in the conduction band by the gap state located at

an energy of E_T. In Equation (7), $e_n(E_T)$ is the corresponding emission rate of electrons. n is the concentration of electron in the conduction band. $f_T(E_T)$ is the fraction of the gap states occupied by electrons at the energy E_T and $\rho(E_T)dE_T$ is the concentration of the gap states located in the energy range E_T and E_T+dE_T. The coefficients in Equations (8) and (9) has the corresponding meanings for holes.

Although the rate equations (6) to (9) are used by Shockley and Read specifically for the thermal transition process, they are also applicable to optical and Auger-impact transition processes using extended definitions for the capture and emission rate coefficients, c_n, c_p, e_n and e_p[5].

The total capture and emission rates through all the gap-state centers can be obtained by summing or integrating Equations (7) to (9) over the distribution of the gap states in the band gap. However, since the gap states are independent, we may apply the condition of steady state to Equations (6) to (9) before making the summation over the gap states. This will be used as an illustration of the modifications of the recombination rates by the presence of a distribution of gap states. Thus, under the d.c. steady-state condition, we have

$$a_T - b_T - c_T + d_T = (\partial_T f_T)/\partial t = 0 \tag{10}$$

which gives the well known Shockley-Read steady-state results

$$F_T(E_T) = \frac{c_n(E_T)N + e_p(E_T)}{c_n(E_T) + e_n(E_T) + c_p(E_T) + e_p(E_T)} \tag{11}$$

$$R_T(E_T) = \frac{c_n(E_T)c_p(E_T)NP - e_n(E_T)e_p(E_T)}{c_n(E_T)N + e_n(E_T) + c_p(E_T)P + e_p(E_T)} \rho_T(E_T)dE_T \tag{12}$$

The total net steady-state recombination rate is then the sum of $R_T(E_T)$ over all the gap states:

$$R_{SS} = \sum R_T(E_T) = \int_{E_V}^{E_C} \frac{c_n(E_T)c_p(E_T)NP - e_n(E_T)e_p(E_T)}{c_n(E_T)N + e_n(E_T) + c_p(E_T)P + e_p(E_T)} \rho_T(E_T)dE_T \tag{13}$$

Here, the integration is from the mobility edges, E_V to E_C, over the density distribution of the gap states, $\rho_T(E_T)$.

Let us now work out a simple example for solar cell junctions which has an explicit result. Consider the forward bias condition in a p-n junction. The constant quasi-Fermi level approximation may be used in the junction space charge layer so that we have

$$PN = n_i^2 \exp(qV/kT) \tag{14}$$

and if we neglect the spatial dependences, then

$$P \simeq N \simeq n_i \exp(qV/2kT) \tag{15}$$

The steady-state recombination rate given by Equation (13) then simplifies to

$$R_{SS} = \frac{n_i(\exp(qV/kT) - 1)}{C\exp(qV/2kT) + 1} \int_{E_V}^{E_C} \frac{e_n(E_T)e_p(E_T)}{e_n(E_T)+e_p(E_T)} \rho_T(E_T)dE_T \tag{16}$$

where the ratio C is somewhat dependent on the properties of the gap states as a function of energy but is assumed to be roughly unity in this example. It is unity if $(c_n+c_p)n_i = e_n+e_p$ at all gap-state energy levels. This is an interesting simple result which shows that the junction current due to recombination in the space charge layer for a distribution of gap states is proportional to the geometrical average of the emission rates over the distribution of the gap states.

2.3 Position Dependent Chemical Composition

For this case, we will consider only the effects from the nonrandom component of the atomic potentials since the gap states produced from the random part can be taken into account by the way described in section II. The fundamental starting point of this problem is the many-body Schroedinger equation for the entire crystal which is assumed to be large so that surface effects are unimportant. Due to position denpendence of the chemical composition, there is a slowly varying aperiodic crystal potential which is the sum of the potentials of all the atoms in the crystal. Then, in the usual manner, the core electrons attached to each atomic nucleus can be taken into account by a transformation [13] to give an effective aperiodic pseudopotential. The aperiodic part can then be isolated out from the periodic part and treated as an extended perturbation to the periodic potential problem. The pseudo-effective mass equation [14] can then be derived for the perturbed problem. Although a detailed mathematical analysis following the above procedure has not been worked out for the specific problem on hand, a simple physical picture emerges which is certainly valid for slowly varying chemical composition. A quantative condition of validity is that the perturbation potential in an extended region under consideration should be small compared with the periodic electric field due to atomic ions in that region. An equivalent condition is that the perturbation potential referenced to an average potential in the extended region should be small compared with the energy gap of interest. For such a slowly varying perturbation, the spatial varation can be represented by the position dependences of the electron affinity, $\chi(\vec{r})$, and energy gap, $E_G(\vec{r})$, or alternatively by the position dependences of the conduction and valence band edges, $E_C(\vec{r})$ and $E_V(\vec{r})$, which serves as the effective potential energies seen by the electrons and holes in the effective mass equations. In

addition, there are also spatial depedences of the density of state or effective masses which must be taken into account. This band model is illustrated in Figure 2.

The equilibrium one-electron distribution function is then given by

$$f(E) = \frac{1}{1 + \exp(E-E_F)/k_BT} \tag{17}$$

where the total energy is the sum of the potential energy and the kinetic energy and E_F is the Fermi energy. In the conduction band, $E > E_C$ and

$$E = E_C + (\hbar^2k^2/2m_C) \tag{18}$$

and in the valence band, $E < E_V$ and

$$E = E_V - (\hbar^2k^2/2m_V) \tag{19}$$

For nonequilibrium, we can define a quasi-Fermi level for electrons, F_N, and one for holes, F_P, so that the distribution functions have the form of

$$f(E) = \frac{1}{1 + \exp(E-E)/k_BT} \tag{20}$$

where $F=F_N$ for electrons and $F=F_P$ for holes. Using the standard perturbation procedure to solve the Boltzmann equation [6] , the modified current equations corresponding to the ideal case given by Equations (1) and (2) are

$$\vec{J}_N = + qD_n\nabla N - q\mu_n N\nabla V_C \tag{21}$$

$$= - q\mu_n N\nabla V_N \tag{21a}$$

and

$$\vec{J}_P = - qD_p\nabla P - q\mu_p P\nabla V_V \tag{22}$$

$$= - q\mu_p P\nabla V_P \tag{22a}$$

where $V_C=-E_C/q$, $V_N=-F_N/q$, $V_V=-E_V/q$ and $V_P=-F_P/q$. For the nondegenerate case, the electron and hole concentrations are given by

$$\begin{aligned} N &= N_C\exp[(E_C-F_N)/k_BT] \\ P &= N_V\exp[(F_P-E_V)/k_BT] \end{aligned} \tag{23}$$

The mobilities and diffusivities appearing in Equations (21) to (22a) are now the local values which are averaged over the carrier concentrations N and P.

In addition, the effective density of states, N_C and N_V, are also local values which are spatially varying due to the position dependences of the density of energy states.

The conventional concepts of an intrinsic sample as well as the intrinsic carrier density and intrinsic Fermi level at thermal equilibrium also lose the familiar meaning since they are functions of the spatial dependences of $E_C(\vec{r})$, $E_V(\vec{r})$, $E_G(\vec{r})$ and $\chi(\vec{r})$. For example, the position dependences of the electrostatic potential for a pure semiconductor, i.e. a graded band gap semiconductor whithout any ionized chemical impurities and defects, can be obtained only by solving the Poisson equation in a given material with known spatial dependences of E_C, E_V, E_G and χ and for specified boundary conditions. This electrostatic potential variation with position, however, will not be the same as the spatial dependences of the intrinsic Fermi potential, $E_I(\vec{r})$, which can still be calculated in the conventional way using Equation (23): $N=P=n_i=\sqrt{N_C N_V}\exp[(E_C-E_V)/k_BT]$ and $F_N=F_P=E_I(\vec{r})$.

The example just given seems unfamiliar at first glance since it defies our firmly-rooted concepts used in semiconductor device analysis. However, further thought on a familiar situation immediately removes this conceptual bottleneck. For example, the different spatial variations between the intrinsic Fermi potential and the electrostatic potential in a graded band gap material has an analogous counterpart in the contact region between two dissimilar but compositional uniform materials such as the oxide-silicon interface in a MOS capacitor. In this case, if we let the electrostatic potential in the oxide coincide with the intrinsic Fermi potential of the oxide and disallow a discontinuity in the electrostatic potential at the interface plane between the oxide and the semiconductor, then the electrostatic potential in the semiconductor will not coincide with the semiconductor intrinsic Fermi potential but will be displaced from it. From this interface picture, one can then readily

build up the spatially varying band picture shown in Figure 2 for a graded gap semiconductor by placing many macroscopically thin semiconductor slices with different chemical compositions in contact. The conclusion on the difference between the electrostatic and intrinsic Fermi potentials is then immediately obvious. Such a multi-layer structure is in fact the model one implicitly uses to solve the one-electron Schroedinger equation as well as the transport equation in a one-dimensional graded gap semiconductor.

A numerical demonstration of the differences between electrostatic and intrinsic Fermi potentials can also be inferred from the work of Emtage which was undertaken many years ago [15].

An important point to be noted is that the electrostatic field, given by the gradient of the electrostatic potential, loses its fundamental microscopic significance in a graded band gap semiconductor. It is the gradient of the conduction or valence band edges, $\nabla E_C(\vec{r})$ and $\nabla E_V(\vec{r})$, which appears in the Schroedinger equation and which give the forces experienced by the electron and hole quasi-particles and <u>not</u> the gradient of the electrostatic potential. This point was made clear by Kroemer [11] who coined these effective fields the quasi-electric fields [16]. Thus, the hot electron properties in a high electric field is dependent on the quasi-electric field for electrons, $\nabla E_C(\vec{r})$, and not the ordinary electrostatic field, ∇V_I, obtained from the Poisson equation. On the other hand, the boundary conditions at an interface between two dissimilar materials are to be imposed on the electrostatic field, electrostatic displacement and electrostatic potential or the true macroscopic charge dnesities, N, P, N_{DD} and N_{AA}, but not on the quasi-electric fields.

2.4 Summary

The modifications of the Shockley equations by the position dependences of the atomic composition of semiconductors are described. Two modifications are analyzed. The first concerns the random spatial variations which give rise to distributions of highly localized states in the band gap. These band gap states enhance the carrier recombination rates. The total steady-state recombination rate at these gap states is worked out as an example and applied to the space charge region of a pn junction.

The second modification discussed in this paper is a major one. It is shown that change in the form appears in the two current equations of the five Shockley equations for a two-band semiconductor. Instead of a proportionality to the conventional electric field, the electron and hole drift currents are now proportional to the gradient of the conduction and valence band edges respectively. These gradients of band edges are also known as the quasi-electric fields and they are not equal in the graded band gap materials while they are equal in an uniform material. The quantum mechanical basis for the presence of the quasi-electric fields are discussed and shown to come from the aperiodic part of the potential energy of the crystal in the many-body problem and its one-electron representation. The use of the quasi-electric fields for hot carrier effects and the electrostatic field for boundary condition matching are also pointed out.

References for Chapter 2

[1] S. M. Sze, Physics of Semiconductor Devices, Wiley, (1969)

[2] A. G. Milnes and D. L. Feucht, Heterojunctions and Metal-Semiconductor Junctions, Academic Press (1972)

[3] W. Shockley, "The theory of p-n junctions in semiconductors and p-n junction transistors", Bell Syst. Tech. J. 28, 435-489 (1949)

[4] W. Shockley, Electrons and Holes in Semiconductors, van Nostrand (1950)

[5] C. T. Sah, "Equivalent circuit models in semiconductor transport for thermal, optical, auger-impact, and tunnelling recombination-generation-trapping processes", physica status solidi a7, 541-559 (1971); see also F. A. Lindholm and C. T. Sah, "Fundamental electronic mechanisms limiting the performance of solar cells", this issue

[6] C. T. Sah and F. A. Lindholm, "Transport in semiconductors with low scattering rate and at high frequencies", Solid-State Electronics, 16, 1447-1449 (1973)

[7] K. Hess and C. T. Sah, "High frequency hot electron conductivity and admittance in Si and Ge", Solid-State Electronics, 18, 667-669 (1975)

[8] M. H. Cohen, H. Fritzsche and S. R. Ovshinsky, "Simple band model for amorphous semiconducting alloys", Phys. Rev. Lett. 22, 1065-1068 (1969)

[9] R. J. van Overstraeden, H. J. deMan and R. P. Mertens, "Transport in heavily doped silicon", IEEE Trans. Ed-20, 290-298 (1973)

[10] C. T. Sah, Excess current in tunnel diodes, Chapter 14 in E. Burstein and S. Lindquist, Tunneling Phenomena in Solids, Plenum Press, N.Y. (1969)

[11] H. Kroemer, "Quasi-electric and quasi-magnetic fields in nonuniform semiconductors" RCA Review 28, 332-342 (1957)

[12] W. Shockley and W. T. Read, "Statistics of recombinations of holes and electrons", Phys. Rev. 87, 835-842 (1952)

[13] J. C. Phillips and L. Kleinman, "New method for calculating wave functions in crystals and molecules", Phys. Rev. 116, 287-294 (1959); V. Hiene, The pseudopotential concept, in Solid State Physics, 24, 1-37 (1970), Edited by Seitz, Turnbull, Academic Press

[14] S. T. Pantelides and C. T. Sah, "Theory of localized states in semiconductors. I. New results using an old method", Phys. Rev. 10, 621-637; "Theory of localized states in semiconductors. II. The pseudo impurity theory application to shallow and deep donors in silicon", Phys. Rev. 10, 638-658, 15 July 1974.

[15] P. R. Emtage, "Electrical conduction and the photovoltaic effect in semiconductors with position-dependent band gaps", J. Appl. Phys. 33, 1950-1960 (1962)

[16] There are also several more recent papers using Kroemer's quasi electric field concept, such as W. G. Oldham and A. G. Milnes, "n-n semiconductor hetrojunctions," Solid-State Electronics, 6, 121-132, (1963) and L. J. Van Ruyven and F. E. Williams, "Electronic transport in graded-band-gap semiconductors," American J. Physics, 35, 705-709 (1967)

Figure Captions

Figure 1 The four electron and hole capture and emission transition processes between a conduction or valence band state and a bound state located at an energy E_T.

Figure 2

(a) The one-electron energy band model of a solid plate with position dependent composition giving rise to spatial variations of the energy gap, E_G, electron affinity, χ, the band edges of the conduction and valence bands, E_C and E_V. The physical crystal potential composed of the sum of the atomic potentials is not shown in the figure. The shaded regions are the conduction and valence bands. Gap states such as those indicated in Figure 1 are not shown here for simplicity. The rise of the potential well (heavy curves) near the crystal surface is highly expanded in relation to the width of the crystal labeled.

(b) The one-electron energy band picture of two semiconductor crystals in contact giving rise to spatial variations of the energy gap, $E_G(y)$, electron affinity, $\chi(y)$, and the conduction and valence band edges, $E_C(y)$ and $E_V(y)$. The two vacuum levels, on the left and right, are shown to illustrate a large area semiconductor plate situation. The dashed $E_C(y)$ and $E_V(y)$ curves with discontinuities are those of the idealized and physically unrealistic situation assumed in the past which overlooked the distortion of the atomic structure and electron distribution in the interface region which give the gradual transition of χ, E_G, E_C and E_V shown in solid curves.

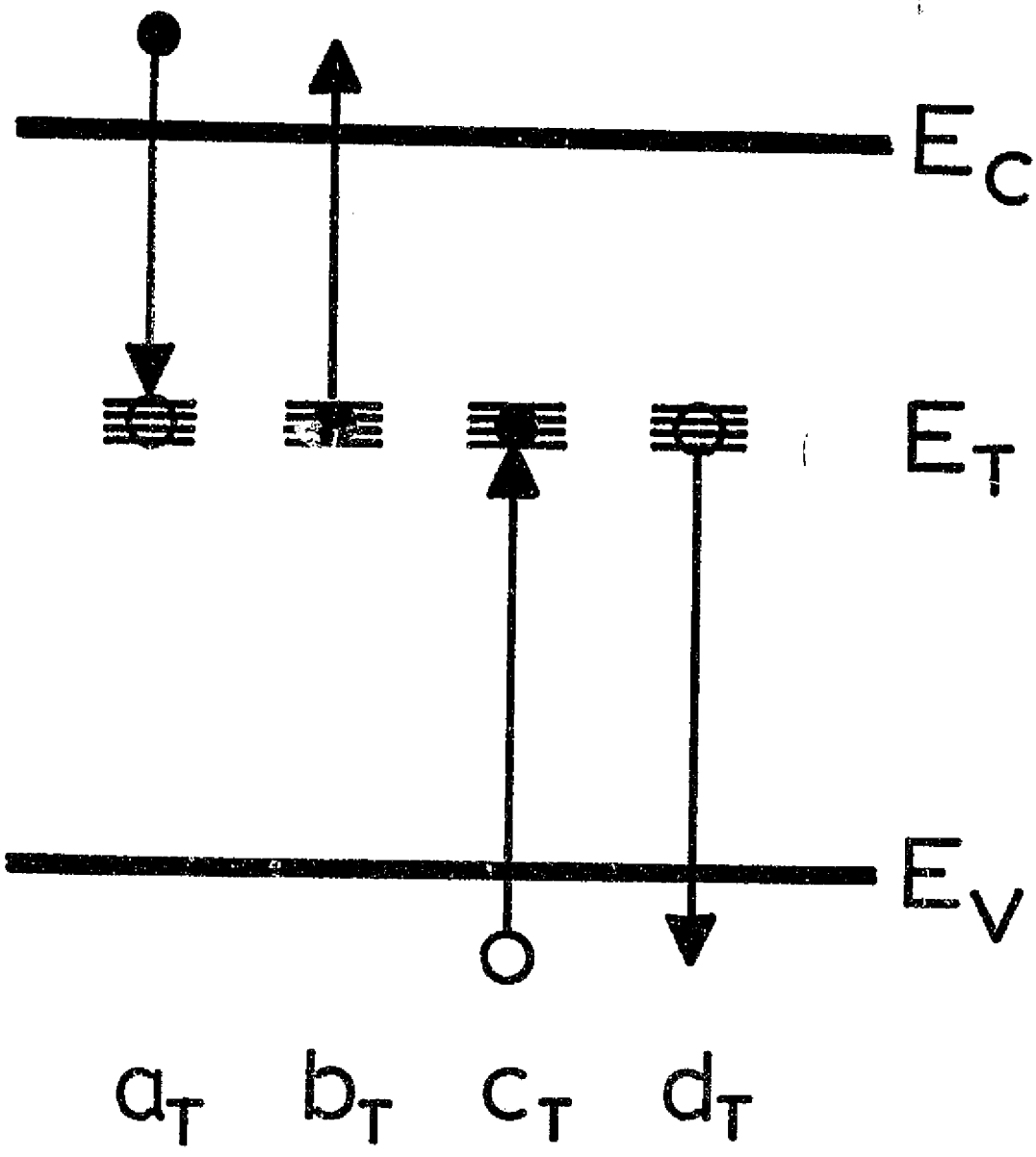

Figure 1

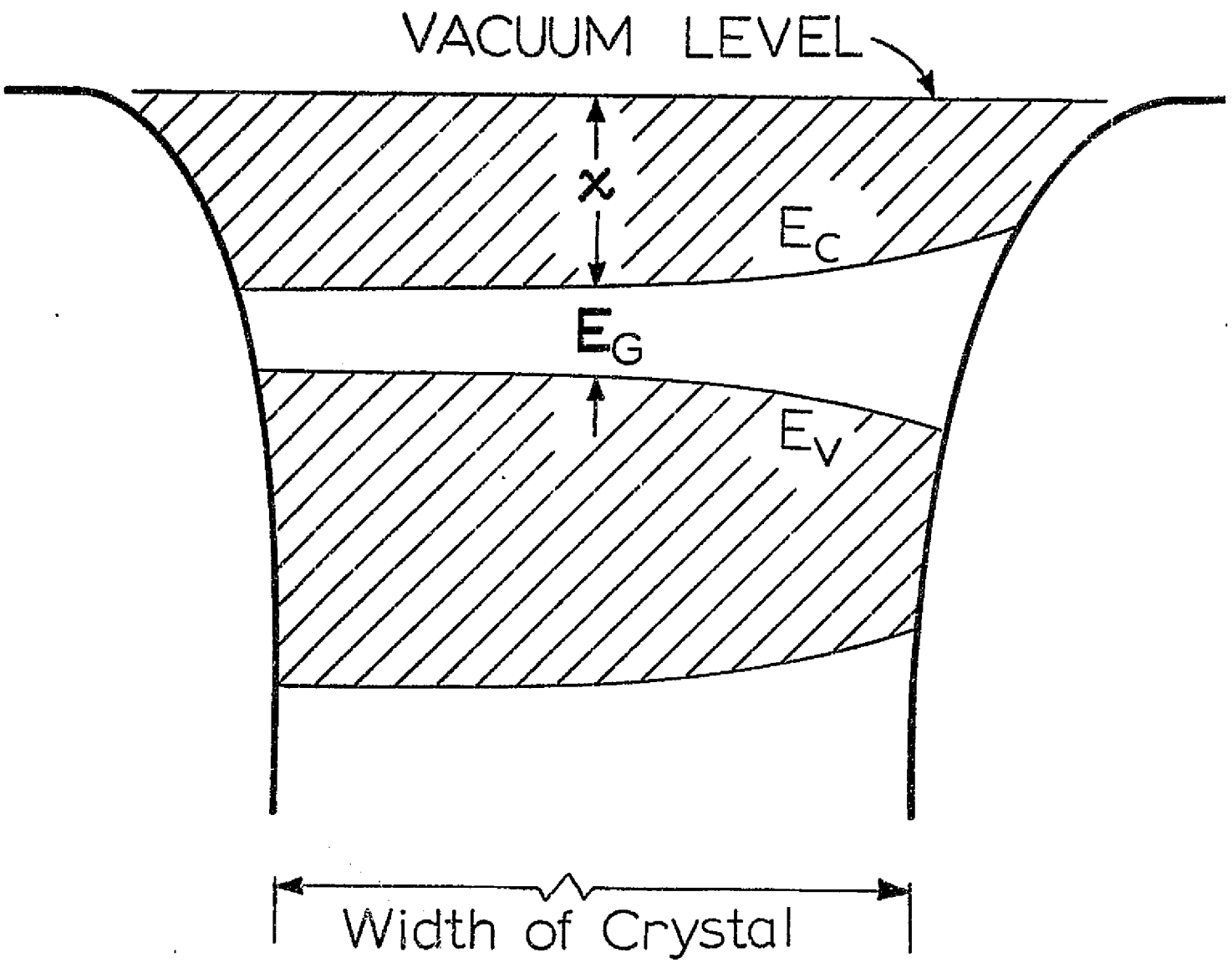

Figure 2 (a)

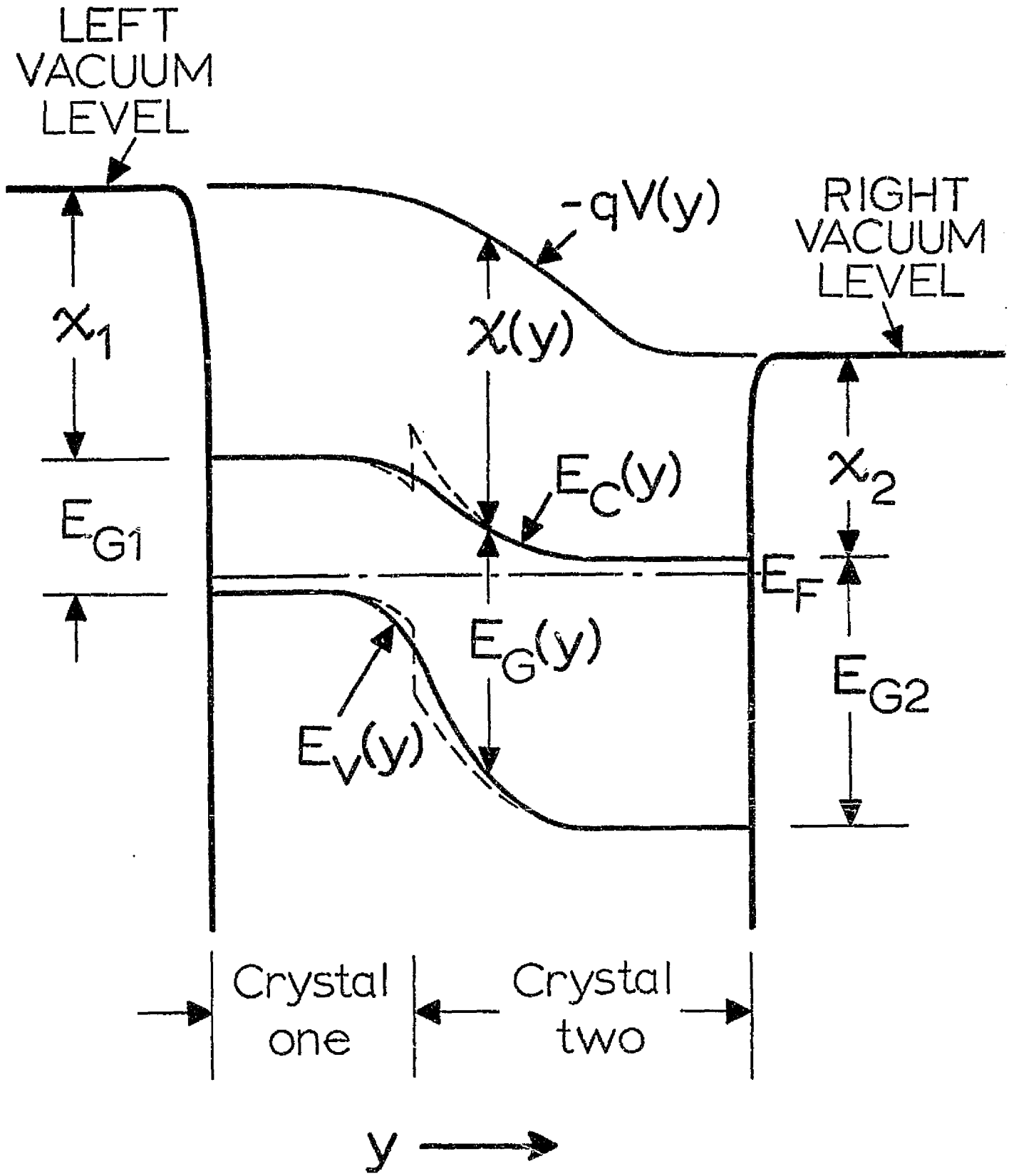
LEFT
VACUUM
LEVEL
-qV(y)
RIGHT
VACUUM
LEVEL
χ_1
$\chi(y)$
$E_C(y)$
χ_2
E_{G1}
E_F
$E_G(y)$
E_{G2}
$E_V(y)$
Crystal
one
Crystal
two
y

Fig. 2(b)

PART II: NEW EXPERIMENTAL METHODS

CHAPTER 3 EXPERIMENTAL DETERMINATION OF SERIES RESISTANCE OF P-N JUNCTION DIODES AND SOLAR CELLS

3.1 Introduction

The series resistance R_s is a parasitic element in diodes and solar cells that can degrade the device performance. In general, the presence of R_s will bend the current-voltage characteristic away from the idealized characteristic [1]. In a solar cell, this bending decreases the power conversion efficiency [2].

The series resistance of a diode or a solar cell consists of the contact resistances of the metal contacts at both faces of the device and of the resistance of the bulk semiconductor. The resistance of the bulk substrate can be calculated taking into account a spreading resistance correction [3]. The contact resistance is difficult to calculate accurately. In solar cells with a very thin diffused layer and contact grid

on the top, the resistance of the diffused layer might dominate. Calculation of this resistance is difficult because of the nonuniform current flow occurring in the diffused layer [4].

Thus, because of the uncertainties and difficulties involved in calculating R_S, methods for direct measurement of R_S are desirable. For a solar cell, a method has been described [5] that involves exposing the solar cell to different illumination levels. Here we describe three other methods for measurement of R_S which can be applied to any diode or solar cell. These methods involve:

a) small signal admittance measurement at moderately high frequency;

b) combined measurement of dc and ac conductance;

c) open-circuit-voltage-decay measurement (OCVD).

3.2 Theory

The small signal equivalent model of the ideal junction diode, derived by Shockley [1], consists of a diode conductance G_{QN} and a diode capacitance C_{QN} in parallel. The circuit elements, G_{QN} and C_{QN}, result from solving the continuity equation for holes and electrons under small signal excitations including both the quasineutral base and emitter regions. In parallel with these two elements, the circuit representation of a real diode includes two capacitances originating in the junction space-charge region: C_T, associated with the ionized impurities, and C_{SCR}, associated

with the mobile charges [6]. The total capacitance is $C_D = C_{QN} + C_T + C_{SCR}$. To complete the circuit, R_s is added, as shown in Figure 1(a).

Method (a): As shown by Sah [6], G_D increases exponentially with increasing bias voltage V_D whereas, for small forward bias, $C_D \simeq C_T$ shows a relatively weak dependence on V_D. If the small-signal admittance of the diode is measured at a forward bias small enough and at a frequency ω high enough that $\omega C_D >> G_D$, then the diode equivalent circuit reduces to R_s and C_D in series, as shown in Fig. 1(b) R_s can then be easily measured using a suitable high-frequency (1 to 10 MHz) bridge.

Method (b): In contrast to method (a), we now set the forward bias voltage V and the frequency ω to such values that $\omega C_D \sim G_D$. Noting that an admittance bridge measures G_p and C_p of the parallel combination shown in Fig. 1(c), we see that the dependence of G_p plotted against V will differ from the dependence of G_D against V because of the presence of R_s. For dc conditions, as illustrated in Fig. 1(d), the measured conductance $G_{DC} = [R_s + 1/G_D]^{-1}$ will show yet another dependence on V. Comparison of $G_p(V,R_s)$ versus $G_{DC}(V,R_s)$ then yields R_s. A simple computer program can be written to enable rapid determination of R_s.

Method (c): The open-circuit-voltage-decay (OCVD) measurement [7] has been often used to determine minority carrier lifetime of a diode. In this measurement, a voltage step applied in the forward direction causes a flow of forward current I.

The terminals are then open-circuited. The resulting cessation of I causes a sharp drop of the voltage ΔV to occur at the diode terminals. This voltage drop ΔV divided by I gives series resistance R_s.

3.3 Results

Table I shows results from methods (a) and (c) together with data obtained by the illumination method of Wolf and Raushenbach [5]. The devices used in the measurements were p^+-n diodes, 30 mil. in diameter and 2x2 cm^2 n^+-p solar cell. The OCVD method was inaccurate for the devices measured since the voltage drop ΔV was difficult to determine accurately; this is especially difficult in devices with short lifetimes. Method (b) could not be used for our devices, since the ac measurements have to be taken at a frequency ω such that $\omega << 2/\tau$ [1], where τ is the minority carrier lifetime in the base. In the devices we studied, τ was a few microseconds which requires measurement at frequencies not exceeding about 1 kHz. At such low frequencies, G_P will differ from G_{DC} by only about 0.005%, which is much less than the estimated experimental accuracy of 1%. This method can be used, however, for short-lifetime devices. For example, if τ = 0.1μsec, the ac measurements could be done at a frequency of a few hundred kHz, at which $G_P - G_{DC}$ would be large enough to enable a determination of R_s.

Method (a) is the simplest approach and gives accurate results that agree reasonably well with those produced by

the illumination method. The accuracy of method (a) is limited by the accuracy of the bridges used, which is better than five percent for the measurements reported here. Measurements were taken at frequencies between 1 and 5 MHz. The results obtained from the illumination method depend on the light intensity [5]; the values of R_s determined by this method fall in the range indicated in Table I. In contrast to the illumination method, method (a) involves only electrical excitation and applies to ordinary diodes as well as to solar cells.

The high-frequency measurements were done on Wayne-Kerr B601 and B801 bridges; low-frequency measurements were done on a Wayne-Kerr B224 bridge.

3.4 Summary

This work demonstrates a simple and rapid method (method (a)) for determining the series resistance of diodes and solar cells based on the measurement of small-signal admittance. The OCVD method (method (c)) provides a rapid but coarse estimate of R_s. Method (b) is useful for devices having a short substrate lifetime. Method (b) enables also measurement of R_s at any bias voltage V, which allows the determination of any dependence that R_s might have on V.

Device	Series resistance R_s in ohms		
	Method (a)	Method (c)	Photovoltaic output [5]
p^+-n diode			
10Ωcm	20	19-28	15-23
p^+-n diode			
0.1Ωcm	4.35	3-10	3.5-4.5
2x2 cm^2 n^+-p solar cell			
2Ωcm	0.33	~0.6	0.25-0.34

Table I Series resistance from methods (a) and (c) together with results using light excitation for comparison.

REFERENCES FOR CHAPTER 3

[1] W. Shockley, "The Theory of p-n junctions in semiconductors and p-n junction transistors," Bell Syst. Tech. J., vol. 28, pp. 435-489, July 1949.

[2] M.B. Prince, "Silicon solar energy converters," J. Appl. Phys., vol. 26, pp. 534-540, May 1955.

[3] G.F. Foxhall and J.A. Lewis, "The resistance of an infinite slab with a dioelectrode," Bell Syst. Tech. J., pp. 1609-1619, July 1964.

[4] R.J. Handy, "Theoretical analysis of the series resistance of a solar cell," Solid-State Electronics, vol. 10, pp. 765-775, 1967.

[5] M. Wolf and H. Raushenbach, "Series resistance effects on solar cell measurements," Advanced Energy Conversion, vol. 3, pp. 455-479, Apr.-June 1963.

[6] C.T. Sah, "Effects of electrons and holes on the transition layer characteristics of linearly graded p-n junction," Proc. IRE, vol. 49, pp. 603-618, March 1961.

[7] S.R. Lederhandler and L.J. Giacoletto, "Measurement of minority carrier lifetime and surface effects in junction devices," Proc. IRE, vol. 43, pp. 477-483, Apr. 1955.

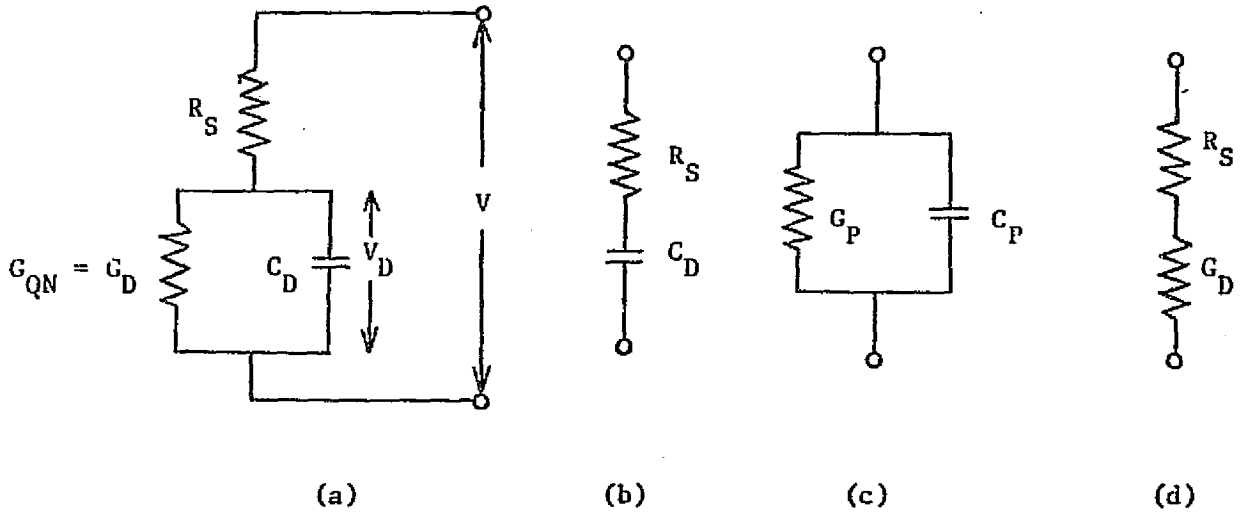

Figure 1 (a) ac equivalent circuit; (b) high-frequency equivalent circuit for $\omega C_D >> G_D$; (c) parallel equivalent circuit as measured by bridge, where G_P, C_P are functions of G_D, C_D, R_S, ω; (d) dc equivalent circuit.

CHAPTER 4 FORWARD-BIAS CAPACITANCE AND CURRENT MEASUREMENTS FOR DETERMINING LIFETIMES AND BAND NARROWING IN P-N JUNCTION SOLAR CELLS

4.1 Introduction

One of the material parameters that most influences the performance of a p-n junction solar cell or diode is the minority-carrier diffusion length L of the base (or substrate) region. The diffusion length limits the collection efficiency and power conversion efficiency achievable in a solar cell, and it controls the current-voltage characteristic in a long-base (nonilluminated) diode.

Many methods exist for the measurement of L. Of these, the ones of most relevance to p-n junction device studies yield the value of L in a solar cell or diode after the junction is formed so that the influence on L of the process used to fabricate the junction is included. Existing measurement methods applicable to this problem [1]-[5] involve various tradeoffs between accuracy and convenience.

The purpose here is to describe a new method [6] applicable to solar cells for measuring L and thus the minority-carrier lifetime τ, which is accurate and requires only straightforward capacitance measurements made at the device terminals. The accuracy results because the measurements required employ very accurate capacitance bridges. The accuracy is demonstrated by showing that the values of L yielded by this capacitance method agree well with those obtained by use of the X-ray method described by Rosenzweig [1]. In contrast, the results determined by the capacitance method disagree sharply with those determined from the open-circuit-voltage-decay method [4], for reasons that are discussed.

In its present form, the method measures L for a non-illuminated cell. We discuss the conditions under which this value of L is appropriate to use in describing an illuminated solar cell, and indicate experiments that confirm these conditions.

The method can also determine material properties of the quasi-neutral emitter region. We discuss the determination of the energy-band narrowing and the phenomenological lifetime in the emitter both by this method and by another method involving only dc measurements of emitter current.

4.2 Theoretical Grounds for the Method

Consider a p^+-n junction diode or solar cell with no illumination applied; analogous results hold for n^+-p devices. The minority-carrier diffusion length, $L_p = \sqrt{D_p \tau_p}$, in the n-type base influences the small-signal capacitance C_{QNB} and conductance G_{QNB} of the quasi-neutral base region according to [7]

$$C_{QNB} = \frac{q}{kT} \frac{Aqn_i^2 L_p}{2N_{DD}} \left[\exp\left(\frac{qV}{kT}\right) - 1\right] \tag{1}$$

$$G_{QNB} = \frac{q}{kT} \frac{Aqn_i^2 D_p}{N_{DD} L_p} \left[\exp\left(\frac{qV}{kT}\right) - 1\right] \tag{2}$$

for an applied sinusoidal signal whose period greatly exceeds the base lifetime τ_p. The above results hold for a one-dimensioanl model of a device having a uniformly doped base and operating under low-injection conditions. The undefined symbols appearing in (1) and (2) have their usual meanings.

If either C_{QNB} or G_{QNB} could be determined from measurements, (1) and (2) would then yield L_p, which is the desired quantity. But the

capacitance C and conductance G measured at the terminals contain components in addition to C_{QNB} and G_{QNB} [8]-[11]

$$C = C_I + C_S + C_{SC} + C_{QNE} + C_{QNB} \tag{3}$$

$$G = G_S + G_{SC} + G_{QNE} + G_{QNB} \tag{4}$$

under low-injection conditions. In (3) and (4) the subscript S refers to the surface region, SC to the junction space-charge region, and QNE and QNB to the quasi-neutral emitter and base regions, respectively. The capacitance C_I is the capacitance due to the ionized impurities in the junction space-charge region and C_{SC} is that due to the mobile holes and electrons in that region [8]. From the viewpoint expressed in (1)-(4), the problem of determining L_p becomes the problem of extracting C_{QNB} from the measured C versus V characteristic or of extracting G_{QNB} from the measured G versus V characteristic.

As experiments [12], [13] including those described in Section III show, G_{QNE} can be comparable to G_{QNB} or larger than G_{QNB} in many p-n junction devices of interest. Thus, except in special cases, one cannot determine G_{QNB}, and hence, L_p, from the conductance data.

The key to the extraction of C_{QNB}, and hence to the determination of L_p, from the C-V data lies in making capacitance measurements at relatively high as well as at low frequencies. At low frequencies, the mobile carriers in all regions of the device respond to the signal, and (3) describes the measured low-frequency capacitance. But, at a higher frequency only mobile carriers associated with C_I and C_S will follow the signal [7] and will contribute to the measured capacitance if the period of the signal is long compared with both the dielectric relaxation

time of the semiconductor and the transit time across the junction space-charge region. Thus by subtracting this higher-frequency capacitance from the low-frequency capacitance, one obtains a capacitance associated with the quasi-neutral regions. This capacitance is C_{QNB} if the phenomenological lifetime τ_E of the emitter [12]-[14] is much shorter than τ_p, and if the signal frequency f is chosen so that $\tau_E \ll 1/f \ll \tau_p$. If, on the other hand, $\tau_E \simeq \tau_p$, or if $1/f \ll \tau_E, \tau_p$, this subtraction yields the capacitance, $C_{QNE} + C_{QNB}$, which reduces to C_{QNB} for the commonly occurring case that $C_{QNE} \ll C_{QNB}$. Thus as will be discussed and illustrated in the following sections, the method yields C_{QNB} and, hence, from (1), the value of L_p.

The method applies directly to large-area solar cells. In some cases, however, advantages may result from making the measurements on small-area test devices. For example, this may be desirable if high-frequency admittance bridges having a suitable capacitance range are unavailable in a particular laboratory. For small-area devices, with radius $a \sim L_p$, the two-dimensional fringing effects illustrated in Fig. 1 invalidate the one-dimensional theory underlying (1) and (2) and corrections must be made. Correction curves were calculated [15] by solving the continuity equation for holes in two space dimensions. One set of correction curves is shown in Fig. 2.

The theory underlying the method, contained in (1) and (2), applies to non-illuminated solar cells. Solar illumination can change the carrier lifetime because the solar spectrum can change the transitional probability rates of the intermediate levels in the forbidden band [16]. In general, the method yields values of lifetime appropriate to an illuminated cell if the shifting approximation holds, that is, if the current under illumina-

tion is the current in the dark shifted by the short-circuit current [17]. Very careful measurements made on various single-crystal silicon p-n junction solar cells demonstrated the applicability of the shifting approximation for AM0 and lower levels of illumination, thus indicating the validity of the method for these cells at these illumination levels. In assessing the applicability of the shifting approximation, corrections may be needed to account for the effects of series resistance.

A quick check for the light-dependence of the lifetime can be made by measuring the forward-biased capacitance in the dark and again with the light on.

4.3 Illustrative Example

To explore the utility of the method, we fabricated a set of small circular p^+-n junction solar cells having various base doping concentrations between 1.4×10^{14} cm^{-3} and 6.5×10^{17} cm^{-3}. Each diode was circular with an area of 4.5×10^{-3} cm^2. Three separate runs were made: runs 1 and 3 at 950°C and run 2 at 1000°C. Runs 1 and 2 employed phosphorus gettering from the back face to getter metallic impurities from the substrate. Boron surface concentration ranged from 1.5×10^{19} cm^{-3} to 4×10^{19} cm^{-3} and the junction depth ranged from 0.3μm to 0.9μm.

Figure 3 shows representative data: the measured $\ell n(G)$ and $\ell n(C)$ dependencies on qV/kT for device from run 1 having a base doping concentration $N_{DD} = 1.25\times10^{15}$ cm^{-3}. The data were taken at 299 K and 376 K. The low-frequency capacitance and conductance, C_{LF} and G_{LF}, were measured at 3 kHz using a Wayne-Kerr B224 bridge. High-frequency capacitance C_{HF} was measured at 10 MHz using a Wayne-Kerr B801B bridge. The level of the ac signal was kept below 5 mV.

To calculate the diffusion length L_p of the base region, we assume that the minority carrier charge storage in the base greatly exceeds that in the emitter, and, hence, that $C_{QNE} << C_{QNB}$. For the particular diode under study, these assumptions are likely to hold for three reasons: a) the low surface concentration N_S tends to limit the size of the energy-gap shrinkage effects [12], [18], [19] in the emitter; b) the low doping concentration N_{DD} of the base implies a large minority carrier charge storage in the base; c) the thinness of the emitter region tends to limit the amount of minority-carrier charge it can store.

$C_{QN} = C_{QNB}$ is obtained by subtracting C_{HF} from C_{LF} which yields for $\ell n\ C_{QN}$ versus qV/kT a straight line having unity reciprocal slope. Then, from (1), the minority carrier diffusion length of the base obtained from the capacitance method is $L_{pC} = 80\mu m$. To assess the accuracy of this result, we also determined the diffusion length by the X-ray method described by Rosenzweig [1], which is accurate within about ±5 percent [1], and found $L_{pX} = 84\mu m$. The good agreement between L_{pC} and L_{pX} tends to confirm the utility and accuracy of the capacitance method.

For some devices, the emitter recombination current will be much less than the base recombination current, so that $G_{QNE} << G_{QNB}$ and L_p can be deduced from (2) using only the low-frequency conductance data. This is true for the device under consideration in Fig. 3. If one assumes $G_{QNE} << G_{QNB}$, one obtains $L_{pG} = 80\mu m$, which agrees well with the values obtained by the capacitance and X-ray methods. G_{QNB} was obtained using a construction technique described elsewhere [13].

But the conductance method fails whenever the emitter recombination current contributes significantly to the current-voltage characteristic, as can be expected to occur in diodes having higher base doping con-

centrations and consequently lower minority-carrier charge storage in the base. This point is illustrated in Fig. 4. For diodes having base doping concentrations above 10^{16} cm^{-3}, L_{pG} differs from L_{pC} and L_{pX} by a factor of two or more. The capcitance and the X-ray methods give results in excellent agreement for all base doping concentrations, however, which illustrates the accuracy and applicability of the capacitance method. Excellent agreement between L_{PC} and L_{PX} also justifies the use of dark C_{QNB} for determination of L_p in solar cells, since X-ray radiation can excite traps in the bandgap in a similar way as light excitation.

For our devices the ratio a/L_p is larger than about 4 and the two-dimensional correction factor is small, as can be seen from Fig. 2. Appropriate corrections were made.

A. Comparison with the Open-Circuit-Voltage-Decay Method

Determination of the base lifetime τ_p by the open-circuit-voltage-decay (OCVD) method [4] is a commonly used approach. The OCVD method is attractive because it involves the measurement of only a single transient, which can be rapidly done.

To examine the applicability of OCVD to silicon devices, we consider first its theoretical basis. In the theoretical development of the OCVD response, one finds the open-circuit response of a diode following the sudden removal of forward bias by solving the continuity equation for the minority carriers in the base. Under low-injection conditions, the open-circuit voltage decays linearly with time, to a close approximation, and measurement of the slope of this straight-line decay suffices to determine τ_p. This result applies if the minority carriers in the base dominate in determining the response, as was the case for the germanium diodes considered in the original OCVD study [4]. But if the carriers associated with the junction

space-charge region or with the quasi-neutral emitter contribute appreciably to the response, then the OCVD method is not applicable.

The junction space-charge region contributes to the measured capacitance and conductance characteristics of Fig. 3, as evidenced by the nonunity slopes of these characteristics, particularly of the capacitance characteristic. At 299 K, the slopes come nearest to unity in the voltage range, $0.45\ V \leq V \leq 0.52\ V$. For this range, the minority hole concentration in the base is in low injection. Figure 5 displays the corresponding OCVD response, taken at 299 K and beginning at $V \simeq 0.5$ V. Note that this response fails to exhibit a simple linear decay. Thus as one could anticipate from the nonideality of conductance and capacitance characteristics, the OCVD method for determining τ_p is inapplicable for this diode at 299 K. A course estimate of τ_p can be inferred from the OCVD response, however, by fitting a straight line to the response and measuring its slope. This yields τ_p (OCVD) $\simeq 8\mu s$, which differs by nearly a factor of two from the value, $\tau_p \simeq 4.4\mu s$, corresponding to $L_{pC} = 80\mu m$ determined by the capacitance method and corroborated by the X-ray method and by the calculation [7], $\tau_p = 2C_{QN}/G_{QN}$. For comparison, the straight-line decay corresponding to $\tau_p = 4.4\mu s$ is plotted on Fig. 5.

According to theory, the quasi-neutral capacitance and conductance increase more rapidly with temperature than do the components from the junction space-charge region. Thus one might expect the capacitance and conductance characteristics to have slopes that more closely approach unity as the temperature is raised. This is confirmed by the data of Fig. 3 measured at 376K, where the closest approach to unity slope occurs in the voltage range, $0.25V < V < 0.32V$. In this range, which corresponds

to low-injection levels of the minority holes in the base, the conductance almost shows an ideal slope of unity, and the capacitance shows a reciprocal slope of 1.07. As Fig. 5 indicates, however, even these slight departures from the ideal characteristics are enough to produce an OCVD response that again fails to exhibit a simple linear decay. The fitting of a straight line to the OCVD response at 376 K results in the estimate τ_p(OCVD) ≈ 9μs, which differs considerably from the value τ_p = 7μs, corresponding to L_{pC} = 80μm at 376K determined by the capacitance method and corroborated by calculation [7], $\tau_p = 2C_{QN}/G_{QN}$.

Similar deviations from the ideal capacitance and conductance characteristics and the ideal (linear) OCVD response were seen for all of the silicon diodes of Fig. 4. This suggests that the OCVD method for determining τ_p is questionable for silicon devices, although one might expect its accuracy to increase as temperature is raised. The capacitance method avoids the inaccuracies resulting from the nonideality of the characteristics by combining low-frequency and high-frequency data.

As was discussed previously [13], the junction current recovery method [20] is generally even a poorer method than OCVD for determining carrier lifetime and diffusion length of the base region.

4.4 Discussion of the Capacitance Method

The capacitance method for determining L_p and τ_p involves measuring the dependence of the capacitance on forward bias at two frequencies: a frequency f_L, low enough that $1/f_L >> \tau_p$, and a frequency f_H high enough that $1/f_H << \tau_p$. Once the low-frequency and higher-frequency capacitance are measured, they are subtracted to give the quasi-neutral capacitance C_{QN}. The resulting dependence of $\ell n(C_{QN})$ on qV/kT must be a straight line of unity slope, which provides a convenient self-consistency check

on the validity of the results. For diodes for which $C_{QNE} \ll C_{QNB}$, which often occurs, the quasi-neutral base capacitance C_{QNB} is thus determined. Combining C_{QNB} with (1) then determines L_p and τ_p.

The inequality, $C_{QNE} \ll C_{QNB}$, holds for the cells of Fig. 4 because the surface doping concentration is low ($N_S \sim 10^{19}$ cm^{-3}) and the emitter junction is thin ($x_j \sim 1$ μm). These conditions make the total number of dopant atoms in the emitter small. That $C_{QNE} \ll C_{QNB}$ for these devices is substantiated by the demonstration that $L_{pC} = L_{pX}$. But if a given device has a large number of dopant atoms in the emitter, then C_{QNE} can be large because of band-narrowing effects [12], [18], [19]. If, in addition, the device has a large doping concentration in the base, which from (1) implies a small value of C_{QNB}, then $C_{QNE} \simeq C_{QNB}$. For such a device, the diffusion length of the base can be determined by the X-ray method, and the method described in this paper can be adapted to enable the determination of the minority-carrier charge Q_E stored in the emitter and the phenomenological lifetime τ_E of the emitter. From the values of Q_E and τ_E thus determined one can deduce information about the band-narrowing and recombination mechanisms in the highly doped emitter [12]. The details of such studies for bipolar transistors were published elsewhere [21], [22]. Similar work on solar cells is in progress.

There are several practical limitations that define the scope of applicability of the capacitance method and they are discussed in detail in Ref. [6]. These limitations are not severe and the capacitance method applies to a wide range of silicon devices, as the results given in Section III demonstrate. The capacitance method has the advantage of being accurate and of requiring only straightforward electrical measurements at the terminal using inexpensive equipment. It also enables the

easy determination of the dependence of diffusion length and lifetime on temperature.

The accuracy of low-frequency capacitance bridges, such as Wayne-Kerr B224, is about ±0.1 percent and the accuracy of available high-frequency bridges is about ±2 percent. If the temperature during measurement is controlled within ±0.1 K, which will introduce an error in n_i^2 less than 2 percent, the overall accuracy of the method is estimated to be about ±5 percent.

4.5 Bandgap Narrowing in Emitter from Temperature Dependence of Emitter Current

Slotboom and deGraaff [23] and Martinelli [24] recently proposed methods to determine bandgap narrowing ΔE_G in the base region of bipolar transistors. Because the base doping of transistors is limited to about 10^{19} cm^{-3}, these methods do not allow investigation of an entire range of high doping densities up to about 10^{21} cm^{-3}. Although these and similar methods provide useful information about bulk material remote from a surface, they cannot directly yield ΔE_G of the thin emitter region of any particular device under study because ΔE_G may depend in part on the proximity of the semiconductor surface near which lattice strain and impurity and defect clustering can occur. In addition, ΔE_G may also depend on the particular diffusion or ion-implantation processing used to form the emitter region.

To determine ΔE_G of the emitter, we propose an alternate method which employs the temperature dependence of the emitter current. This method applies over the entire range of emitter doping concentrations present in p-n junction devices. If the emitter doping profile is flat, the interpretation of the results of the method is particularly straightforward.

The simplest version of the method results if the emitter is transparent, i.e., if injected holes (for an n^+-p device) recombine mainly at the surface rather than in the bulk of the emitter. If the emitter region is thin, the transparency of the emitter can be demonstrated experimentally even for very high emitter doping concentrations. A theoretical and experimental discussion of this issue will appear elsewhere.

If the emitter is transparent and if the surface recombination velocity S_p is large, then [25]

$$J_{EO} = q\left[\int_0^{W_E} \frac{N(x)}{D_p(x)n_{ie}^2(N)}\,dx\right]^{-1} \tag{5}$$

where $n_{ie}^2 = CT^3\exp(-E_{GO}(N)/kT)$ in which C is a constant nearly independent of the doping concentration [23]. $E_{GO}(N)$ is the bandgap extrapolated to 0 K, which equals 1.206 eV for low doping concentrations [23,26]. For a degenerately-doped emitter region, in which the electron concentration N is large, the mobility is assumed to be independent of temperature. The quasineutral emitter thickness is W_E. In (5), n_{ie}^2 is the effective intrinsic density.

For a flat doping profile, (5) becomes

$$J_{EO} = C_1 T^4 \exp(-E_{GO}(N)/kT) \tag{6}$$

where C_1 is independent of temperature.
Thus a plot of $\ln(J_{EO}/T^4)$ versus 1/T yields a straight line from which $E_{GO}(N)$ can be calculated. The emitter saturation current J_{EO} is determined from the measured total saturation current by techniques described elsewhere [12,13].

The method was used to measure E_G on a device with almost flat implanted As profile with $N \simeq 1.5 \times 10^{20}$ cm^{-3} and $W_E \simeq 0.37\mu m$. The plot of $\ell n(J_{EO}/T^4)$ versus $1/T$ for this device appears in Fig. 6. From the slope $E_{GO} = 1.046$ eV which gives $\Delta E_{GO} = 1.206$ eV - 1.046 eV = 0.160 eV.

Additional points for the entire range of emitter dopings from 10^{17} cm^{-3} to 10^{21} cm^{-3} are being measured and adjusted to include the effects of Fermi-Dirac statistics. The results will be published elsewhere.

REFERENCES FOR CHAPTER IV

1. W. Rosenzweig, Bell Syst. Tech. J., 41, 1573-1588 (1962).

2. J.H. Lamneck, Jr., NASA Tech. Rep. TMX-1894 (1969).

3. J.H. Reynolds and A. Meulenberg, J. Appl. Phys., 45, 2582-2592 (1974).

4. S.R. Lederhandler and J.J. Giacoletto, Proc. IRE, 43, 447-483 (1955).

5. E.D. Stokes and T.L. Chu, Tech. Dig. of 1976 Int. Electron Devices Meet., 478-479 (1976).

6. A. Neugroschel, P.J. Chen, S.C. Pao, and F.A. Lindholm, IEEE Trans. Electron Devices, ED-25, 485-490 (1978).

7. W. Shockley, Bell Syst. Tech. J., 28, 435-489 (1949).

8. C.T. Sah, Proc. IRE, 49, 603-618 (1961).

9. H. Maes and C.T. Sah, IEEE Trans. Electron Devices, ED-23, 1131-1143 (1976).

10. C.T. Sah, R.N. Noyce, and W. Shockley, Proc. IRE, 45, 1228-1243 (1957).

11. C.T. Sah, IRE Trans. Electron Devices, ED-9, 94-108 (1962).

12. F.A. Lindholm, A. Neugroschel, C.T. Sah, M.P. Godlewski, and H.W. Brandhorst, IEEE Trans. Electron Devices, ED-24, 402-410 (1977).

13. A. Neugrsochel, F.A. Lindholm, and C.T. Sah, IEEE Trans. Electron Devices, ED-24, 662-671 (1977).

14. F.A. Lindholm and C.T. Sah, J. Appl. Phys., 47, 4203-4205 (1976).

15. P.J. Chen, Ph.D. Thesis, Univ. of Florida (1978).

16. C.T. Sah, IEEE Trans. Electron Devices, ED-24, 410-419 (1977).

17. F.A. Lindholm, J.G. Fossum, and E.L. Burgess, "Application of the superposition principle to solar cell analysis," IEEE Trans. Electron Devices, 1978.

18. F.A. Lindholm and C.T. Sah, IEEE Trans. Electron Devices, ED-24, 299-304 (1977).

19. C.T. Sah and F.A. Lindholm, IEEE Trans. Electron Devices, ED-24, 358-362 (1977).

20. R.H. Kingston, Proc. IRE, 42, 829-834 (1954). H.J. Kuno, IEEE Trans. Electron Devices, ED-11, 8-14 (1964).

21. A. Neugroschel, C.T. Sah, and F.A. Lindholm, IEEE Trans. Electron Devices, ED-24, 1362-1365 (1977).

22. M.S. Birrittella, M.S. Thesis, Univ. of Florida (1978).

23. J.W. Slotboom and H.C. deGraaff, Solid-State Electronics, 19, 857-862 (1976).

24. R.U. Martinelli, IEEE Trans. Electron Devices, ED-23, 1218 (1976).

25. H.J. DeMan, IEEE Trans. Electron Devices, ED-18, 833-835 (1971).

26. G.G. MacFarlane, J.P. McLean, J.E. Quarrington, and V. Roberts, Phys. Rev., 111, 1245 (1958).

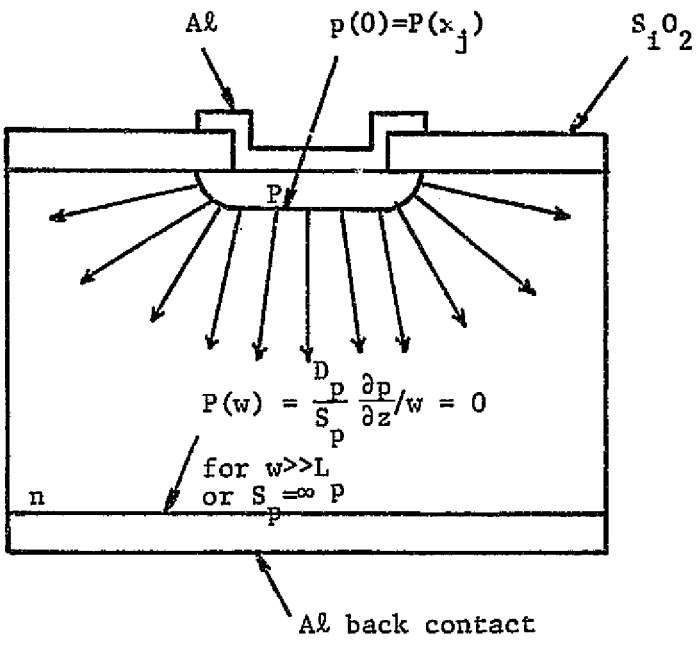

Fig. 1 Cross-section of a diffused p^+-p junction diode showing a two-dimensional spreading effect. Boundary conditions for hole concentrations at the junction edge $P(x_j)$ and at the back contact P(W) are indicated. W is the base width and S_p is a surface recombination velocity at the back contact.

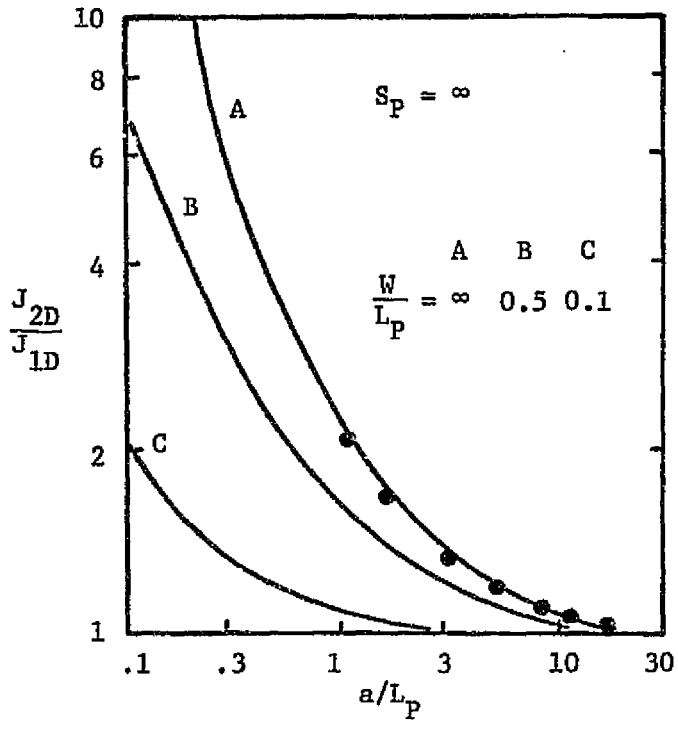

Fig. 2 Ratio of two-dimensional current density J_{2D} to one-dimensional current density J_{1D} as a function of the ratio of device radius a and diffusion length L_p.

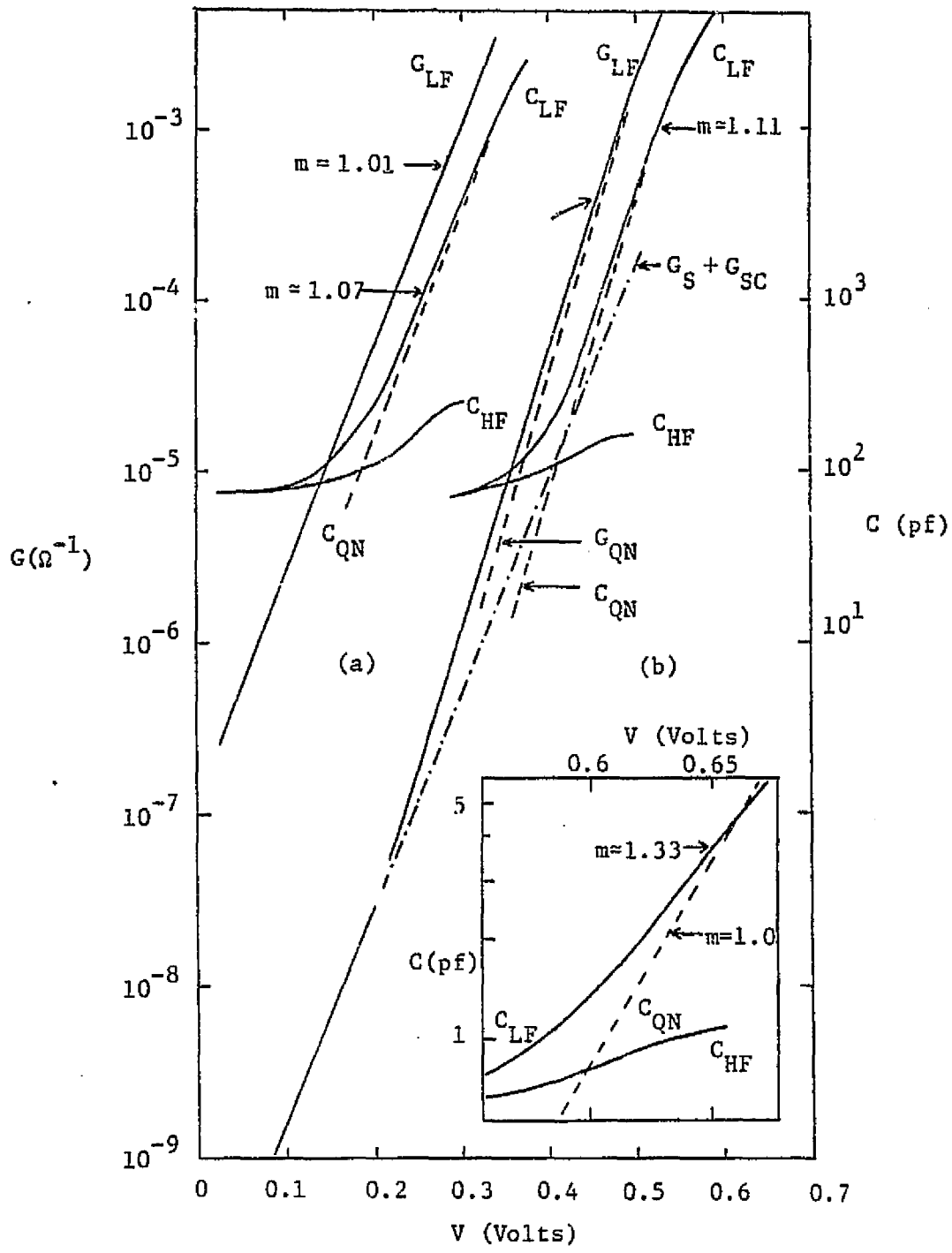

Fig. 3 Measured conductance and capacitance versus forward bias V for diode with $N_{DD} = 1.25 \times 10^{15}$ cm^{-3}. a T=376 K; b T=299K. The insert shows the capacitance characteristic for diode with $N_{DD}=8 \times 10^{16}$ cm^{-3}, demonstrating the increased importance of C_{SC} and emphasizing the value of the subtraction for determining C_{QNB}. In the figure, ---- stands for the components from the quasi-neutral regions (m=1) and -.-.-. stands for $G_{SC} + G_S$.

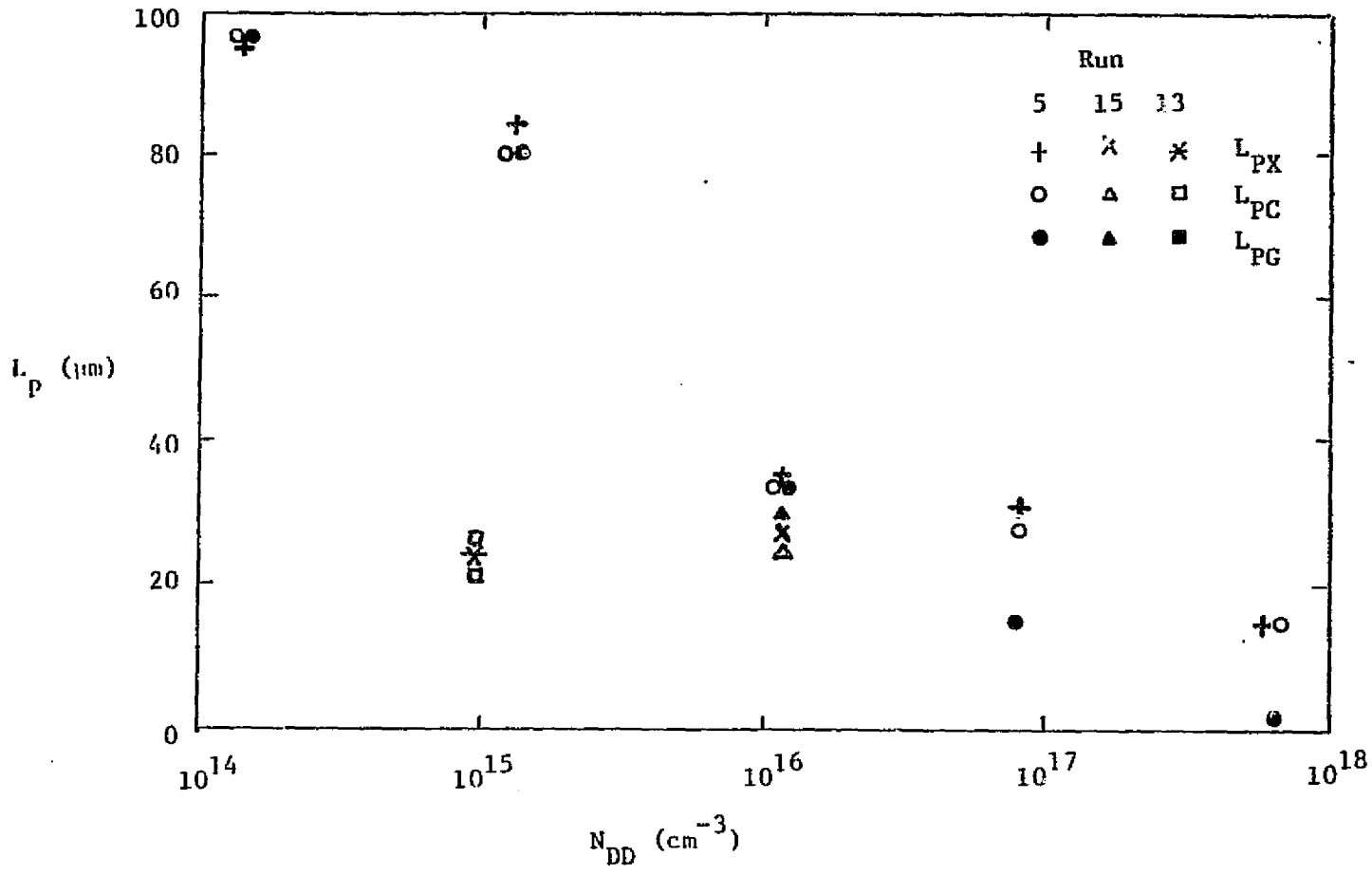

Fig. 4 Diffusion length L_p determined by capacitance, conductance, and X-ray methods versus base doping concentration N_{DD}.

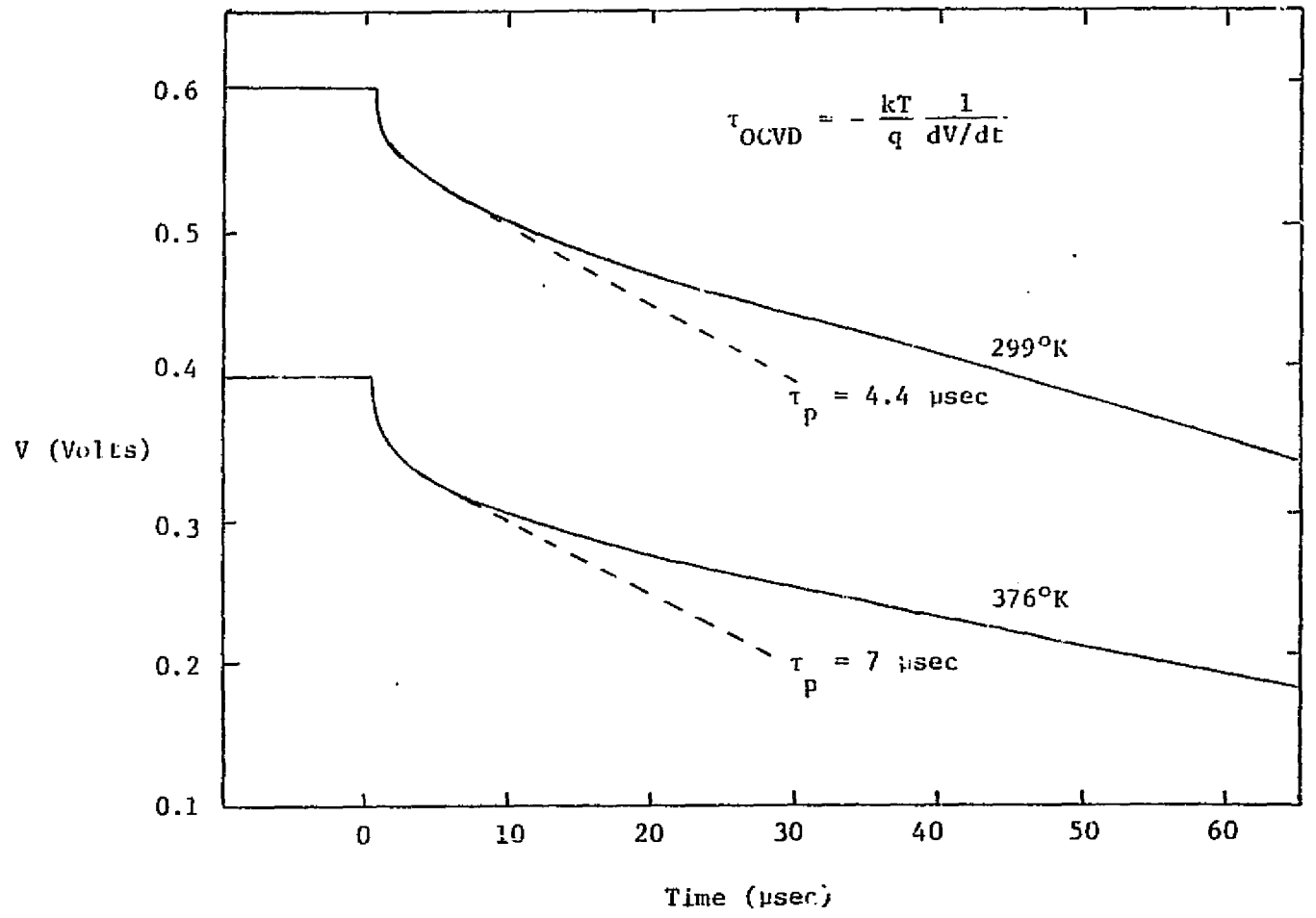

Fig. 5 OCVD response for device of Fig. 3 at 299 K and 376 K. Dashed lines correspond to the lifetime τ_p determined by the capacitance method.

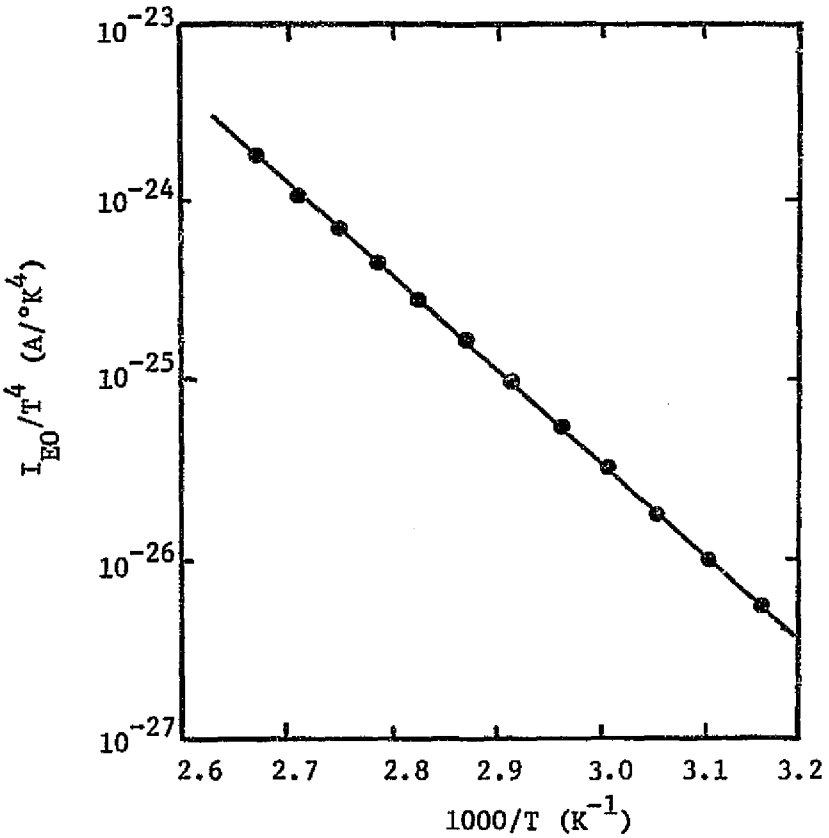

Fig. 6 $\ell n(I_{EO}/T^4)$ versus 1000/T with a slope giving E_{GO} = 1.046 eV for $N_D \simeq 1.5 \times 10^{20}$ cm^{-3}.

CHAPTER 5

AN ANALYSIS OF THE DIFFUSION CURRENT AND CAPACITANCE IN A TWO DIMENSIONAL p-n JUNCTION DIODE FOR DETERMINING THE DIFFUSION LENGTH

5.1 Introduction

In a previous related publication [1] by the authors a method was proposed for determining the diffusion length in the base of a p-n junction diode from measurements of the diffusion current-voltage and diffusion capacitance-voltage characteristics. As a central approximation in the development of this method, the current and capacitance characteristics were assumed to be those resulting from the conventional one-dimensional model of the diode, in which excess hole and electron distributions are adequately described by a single space variable x, the distance from the junction surface. This approximation describes the characteristics with sufficient accuracy if the area is large, or more precisely, for a circular device, if the radius a of the emitter region greatly exceeds the minority-carrier diffusion length L_p of the base region. But the bridge used for the high-frequency capacitance measurements required in this method imposes an upper limit on the capacitance that can be measured. Thus diode structures must sometimes be used for which the approximation is invalid and for which the one-dimensional model of the diode introduces intolerable error in the determination of L_p. Figure 5.1

illustrates a p-n junction diode that, if L_p were large enough, would be poorly described by a one-dimensional model.

The purpose of this chapter is to provide an analysis of the diffusion current and capacitance characteristics for a two-dimensional model of the p-n junction diode that allows the determination of L_p for any value of a/L_p.

Grimbergen [2] has treated a problem related to the one of interest. Grimbergen studied a p-n-n^+ structure. He assumed the surface recombination velocity S_p at the high-low n-n^+ junction to be zero and the base width W to be much smaller than L_p. Grimbergen reduced the two-dimensional problem to two coupled one-dimensional problems. As will be shown, the result he obtained is close to one of the cases of our two-dimensional calculation, that corresponding to $S_p = 0$, and $\frac{W}{L_p} = 0.1$ in Fig. 5.2. But, for many diodes, the assumption $S_p = 0$ at the back face is inappropriate and the ratio W/L_p is not necessarily small. Thus, a general solution of two-dimensional problems will be useful.

The chapter begins by defining the boundary-value problem. It resembles boundary-value problems encountered in the conduction of heat but differs in that a volume recombination term appears in the differential equation. The solution of this boundary-value problem is then presented, which yields the current $I(\alpha)$ and the capacitance $C(\alpha)$ normalized by their one-dimensional counterparts plotted against the ratio, $\alpha = a/L_p$. Used in conjunction with current and capacitance measurements, the plot enables the determination of L_p. This is illustrated for two devices with different areas. The diffusion length L_p determined by this method is shown to be consistent with that determined

by the X-ray method [3] which illustrates the good accuracy to be expected from use of the two-dimensional analysis.

5.2 Theoretical Analysis

The hole diffusion problem in the n-type substrate of a shallow diffused p-n junction (see Fig. 5.1) is similar to the heat conducting problem of a metal disk [4,5], except that a volume recombination term appears in the differential equation, describing the kinetics of the holes. The differential equation originates from the continuity equation, which for the steady-state condition is

$$\nabla \cdot J_p = -qP'/\tau_p \tag{5.1}$$

with

$$J_p = -qD_p \nabla P \tag{5.2}$$

Combining (5.1) and (5.2) yields

$$\nabla^2 P = \frac{P'}{D_p \tau_p} = \frac{P'}{L_p^2} \tag{5.3}$$

where $P' = P - P_{no}$ is the excess hole concentration and $L_p = \sqrt{D_p \tau_p}$ is the diffusion length of holes in the base region. In cylindrical coordinate (ρ,ϕ,z), equation (5.3) becomes

$$\frac{\partial^2 P'}{\partial \rho^2} + \frac{1}{\rho}\frac{\partial P'}{\partial \rho} + \frac{1}{\rho^2}\frac{\partial^2 P'}{\partial \phi^2} + \frac{\partial^2 P'}{\partial z^2} = \frac{P'}{L_p^2} \tag{5.4}$$

Separation of variables is accomplished by substituting $P'(\rho,\phi,z) = R(\rho)\Phi(\phi)Z(z)$, which leads to

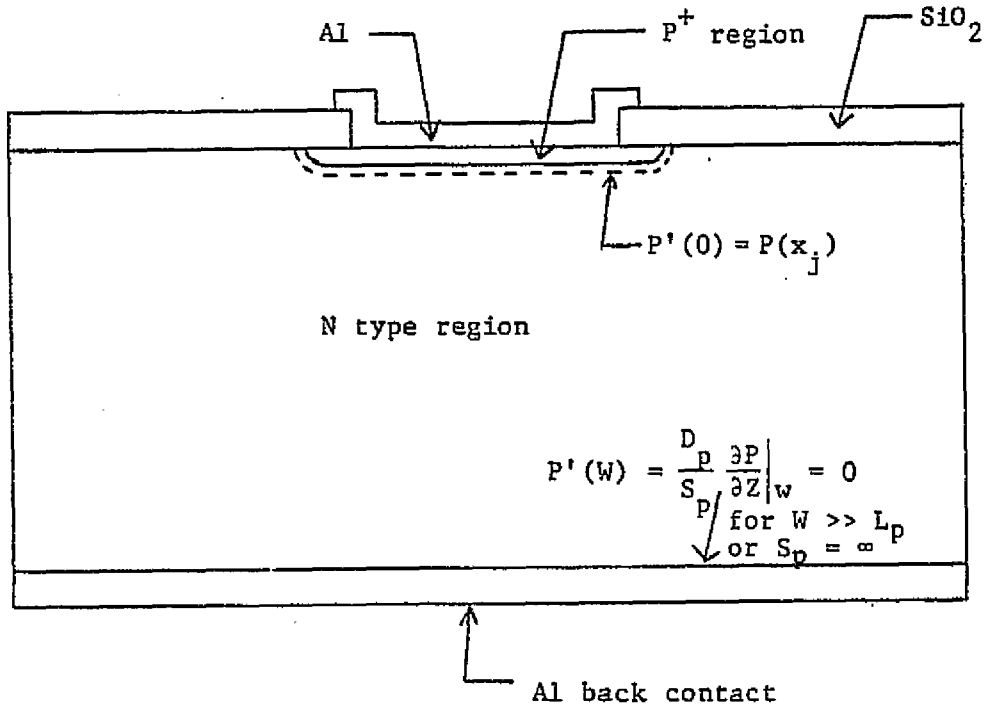

Figure 5.1 Cross-section of a shallow diffused p^+-n junction diode.

$$\frac{1}{R}\frac{\partial^2 R}{\partial \rho^2} + \frac{1}{R\rho}\frac{\partial R}{\partial \rho} + \frac{1}{\Phi}\frac{1}{\rho^2}\frac{\partial^2 \Phi}{\partial \phi^2} + \frac{1}{Z}\frac{\partial^2 Z}{\partial z^2} - \frac{1}{L_p^2} = 0 \tag{5.5}$$

Normalization with respect to the junction radius a can be done by introducing $\rho = ra$. Thus, equation (5.5) becomes

$$\frac{1}{R}\frac{\partial^2 R}{\partial r^2} + \frac{1}{Rr}\frac{\partial R}{\partial r} + \frac{1}{\Phi}\frac{1}{r^2}\frac{\partial^2 \Phi}{\partial \phi^2} + \frac{a^2}{Z}\frac{\partial^2 Z}{\partial z^2} - \frac{a^2}{L_p^2} = 0 \tag{5.6}$$

Now, let

$$\frac{a^2}{Z}\frac{\partial^2 Z}{\partial z^2} - \frac{a^2}{L_p^2} = k^2 \tag{5.7}$$

$$\frac{1}{\Phi}\frac{\partial^2 \Phi}{\partial \phi^2} = -\nu^2 \tag{5.8}$$

and

$$\frac{a}{L_p} = \alpha \tag{5.9}$$

Substituting (5.7) and (5.8) into (5.6), we obtain

$$\frac{d^2 R}{dr^2} + \frac{1}{r}\frac{dR}{dr} + \left(k^2 - \frac{\nu^2}{r^2}\right)R = 0 \tag{5.10}$$

For a problem possessing azimuthal symmetry, $\nu = 0$, i.e., Φ = constant. Thus, (5.6) reduces to the two ordinary differential equations (5.7) and (5.10). Solutions of (5.7) and (5.10) are

$$Z = A\, e^{-\frac{\sqrt{k^2 + \alpha^2}}{a} z} + B\, e^{\frac{\sqrt{k^2 + \alpha^2}}{a} z} \tag{5.11}$$

$$R = CJ_0(kr) \tag{5.12}$$

Therefore, we have

$$P'(r,z) = \sum_{k=0}^{\infty} R \cdot Z = \sum_{k=0}^{\infty} \left(A\, e^{-\frac{\sqrt{k^2+\alpha^2}}{a} z} + B\, e^{\frac{\sqrt{k^2+\alpha^2}}{a} z}\right) J_0(kr) \qquad (5.13)$$

For a diode with base width W and a surface recombination velocity S_p at the back contact (x = W), the boundary condition at z = W requires that

$$D_p \left.\frac{\partial P'(r,z)}{\partial z}\right|_{z=W} = -S_p \left. P'(r,z)\right|_{z=W} \qquad (5.14)$$

The negative sign in (5.14) is defined by the current direction. Substituting (5.13) into (5.14), for any number of k, we have

$$D_p\left[(-A)\cdot\frac{\sqrt{k^2+\alpha^2}}{a} e^{-\frac{\sqrt{k^2+\alpha^2}}{a} W} + B\cdot\frac{\sqrt{k^2+\alpha^2}}{a} e^{\frac{\sqrt{k^2+\alpha^2}}{a} W}\right] = -S_p\left[A\, e^{-\frac{\sqrt{k^2+\alpha^2}}{a} W} + B\, e^{\frac{\sqrt{k^2+\alpha^2}}{a} W}\right] \qquad (5.15)$$

From (5.15) we obtain

$$B = \frac{1 - \frac{D_p}{S_p}\cdot\frac{\sqrt{k^2+\alpha^2}}{a}}{1 + \frac{D_p}{S_p}\cdot\frac{\sqrt{k^2+\alpha^2}}{a}} \cdot e^{-\frac{\sqrt{k^2+\alpha^2}}{a} 2W} \cdot (-A) \qquad (5.16)$$

Substituting (5.16) into (5.13), we have

$$P'(r,z) = \sum_{k=0}^{\infty} A\left[e^{-\frac{\sqrt{k^2+\alpha^2}}{a}z} - \frac{1-\frac{D_p}{S_p}\cdot\frac{\sqrt{k^2+\alpha^2}}{a}}{1+\frac{D_p}{S_p}\cdot\frac{\sqrt{k^2+\alpha^2}}{a}} e^{-\frac{\sqrt{k^2+\alpha^2}}{a}2W} e^{\frac{\sqrt{k^2+\alpha^2}}{a}z}\right] J_0(kr)$$

$$= \int_0^{\infty} A(k)\left[e^{-\frac{\sqrt{k^2+\alpha^2}}{a}z} - \frac{1-\frac{D_p}{S_p}\cdot\frac{\sqrt{k^2+\alpha^2}}{a}}{1+\frac{D_p}{S_p}\cdot\frac{\sqrt{k^2+\alpha^2}}{a}} e^{-\frac{\sqrt{k^2+\alpha^2}}{a}2W} e^{\frac{\sqrt{k^2+\alpha^2}}{a}z}\right] J_0(kr)\,dk \qquad (5.17)$$

For a shallow diffused junction diode, with zero surface recombination velocity at the front side of $Si-SiO_2$ interface, the boundary conditions require that

$$P'(r,0) = P'(x_j) = \int_0^{\infty} A(k)\left[1 - \frac{1-\frac{D_p}{S_p}\cdot\frac{\sqrt{k^2+\alpha^2}}{a}}{1+\frac{D_p}{S_p}\cdot\frac{\sqrt{k^2+\alpha^2}}{a}} e^{-\frac{\sqrt{k^2+\alpha^2}}{a}2W}\right] J_0(kr)\,dk \qquad (5.18)$$

for $0 < r < 1$

and

$$\frac{\partial' P(r,0)}{\partial z} = 0 = \int_0^{\infty} (-)A(k)\frac{\sqrt{k^2+\alpha^2}}{a}\left[1 + \frac{1-\frac{D_p}{S_p}\cdot\frac{\sqrt{k^2+\alpha^2}}{a}}{1+\frac{D_p}{S_p}\cdot\frac{\sqrt{k^2+\alpha^2}}{a}} e^{-\frac{\sqrt{k^2+\alpha^2}}{a}2W}\right] J_0(kr)\,dk \qquad (5.19)$$

for $1 < r < \infty$

Such pairs of integral equations are known as "Dual Integral Equations" [6]. We now compare (5.18) and (5.19) with the following integral pairs:

$$\int_0^{\infty} G(k)f(k)J_0(kr) = Ar^0 = A \qquad 0 < r < 1 \qquad (5.20)$$

and

$$\int_0^\infty f(k)J_0(kr) = 0 \qquad 1 < r < \infty \tag{5.21}$$

Thus

$$f(k) = A(k)\sqrt{k^2+\alpha^2}\left[1 + \frac{1-\frac{D_p}{S_p}\cdot\frac{\sqrt{k^2+\alpha^2}}{a}}{1+\frac{D_p}{S_p}\cdot\frac{\sqrt{k^2+\alpha^2}}{a}} e^{-\frac{\sqrt{k^2+\alpha^2}}{a}2W}\right] \tag{5.22}$$

and

$$G(k) = \frac{1}{\sqrt{k^2+\alpha^2}}\cdot\frac{\left[1-\frac{1-\frac{D_p}{S_p}\cdot\frac{\sqrt{k^2+\alpha^2}}{a}}{1+\frac{D_p}{S_p}\cdot\frac{\sqrt{k^2+\alpha^2}}{a}} e^{-\frac{\sqrt{k^2+\alpha^2}}{a}2W}\right]}{\left[1+\frac{1-\frac{D_p}{S_p}\cdot\frac{\sqrt{k^2+\alpha^2}}{a}}{1+\frac{D_p}{S_p}\cdot\frac{\sqrt{k^2+\alpha^2}}{a}} e^{-\frac{\sqrt{k^2+\alpha^2}}{a}2W}\right]} \tag{5.23}$$

If we choose

$$f(k) = k^{1/2}\sum_{m=0}^{\infty} a_m J_{2m+\frac{1}{2}}(k) \tag{5.24}$$

a_m can be determined from the following simultaneous equations:

$$\begin{aligned} a_o + \sum_{m=0}^{\infty} L_{m\cdot o}a_m &= \sqrt{\frac{2}{\pi}}\,P(x_j) \quad \text{for } n = 0 \\ a_n + \sum_{n=0}^{\infty} L_{m\cdot n}a_n &= 0 \qquad\qquad \text{for } n > 0 \end{aligned} \tag{5.25}$$

where

$$(4n+1)^{-1}L_{m\cdot n} = \int_0^\infty [kG(k) - 1]\frac{1}{k}J_{2m+\frac{1}{2}}(k)\,J_{2n+\frac{1}{2}}(k)\,dk \tag{5.26}$$

Numerical methods are used in computing $L_{m\cdot n}$.

Once a_m is determined, the total hole diffusion current across the junction is

$$I = qD_p \int_0^a \frac{\partial P'(r,0)}{\partial z} 2\pi\rho d\rho = qD_p a^2 \int_0^1 \frac{\partial P'(r,0)}{\partial z} 2\pi r dr$$

$$= qD_p a^2 \int_0^1 \int_0^\infty k^{1/2} \frac{1}{a}\left[\sum_{m=0}^{\infty} a_m J_{2m+\frac{1}{2}}(k)\right] J_0(kn) 2\pi r dr \qquad (5.27)$$

After integrating (5.27) and dividing it by the one-dimensional current I_0, which can be expressed as

$$I_0 = \frac{qD_p}{L_p} \cdot \pi a^2 P'(x_j) \left[\frac{(\frac{S_p L_p}{D_p})\cosh(\frac{W}{L_p}) + \sinh(\frac{W}{L_p})}{(\frac{S_p L_p}{D_p})\sinh(\frac{W}{L_p}) + \cosh(\frac{W}{L_p})} \right] \qquad (5.28)$$

the ratio of I_α/I_0 appears as plotted as a function of α in Fig. 5.2. In this figure, W/L_p and $S_p L_p/D_p$ are parameters.

For a long-base diode, i.e., one for which $W >> L_p$, the constant B in (5.16) approaches zero. For this case, the detailed solution of the two-dimensional boundary value problem is given in Appendix II of Ref. [7]. The result is [8,9]

$$f(\alpha) = \frac{I_\alpha}{I_0} = \frac{J_\alpha}{J_0} = \frac{4}{\pi\alpha} (A_0 + 0.A_1 + 0.A_2 + \ldots) = \frac{4}{\pi\alpha} A_0 \qquad (5.29)$$

Because the series $\sum_{m=0}^{\infty} A_m$ converges fast, neglecting terms higher than A_2 yields I_α/I_0 to an accuracy of $\pm 3\%$. The same procedures can be applied to calculate $f(\alpha)$ for different values of W/L_p and $S_p L_p/D_p$.

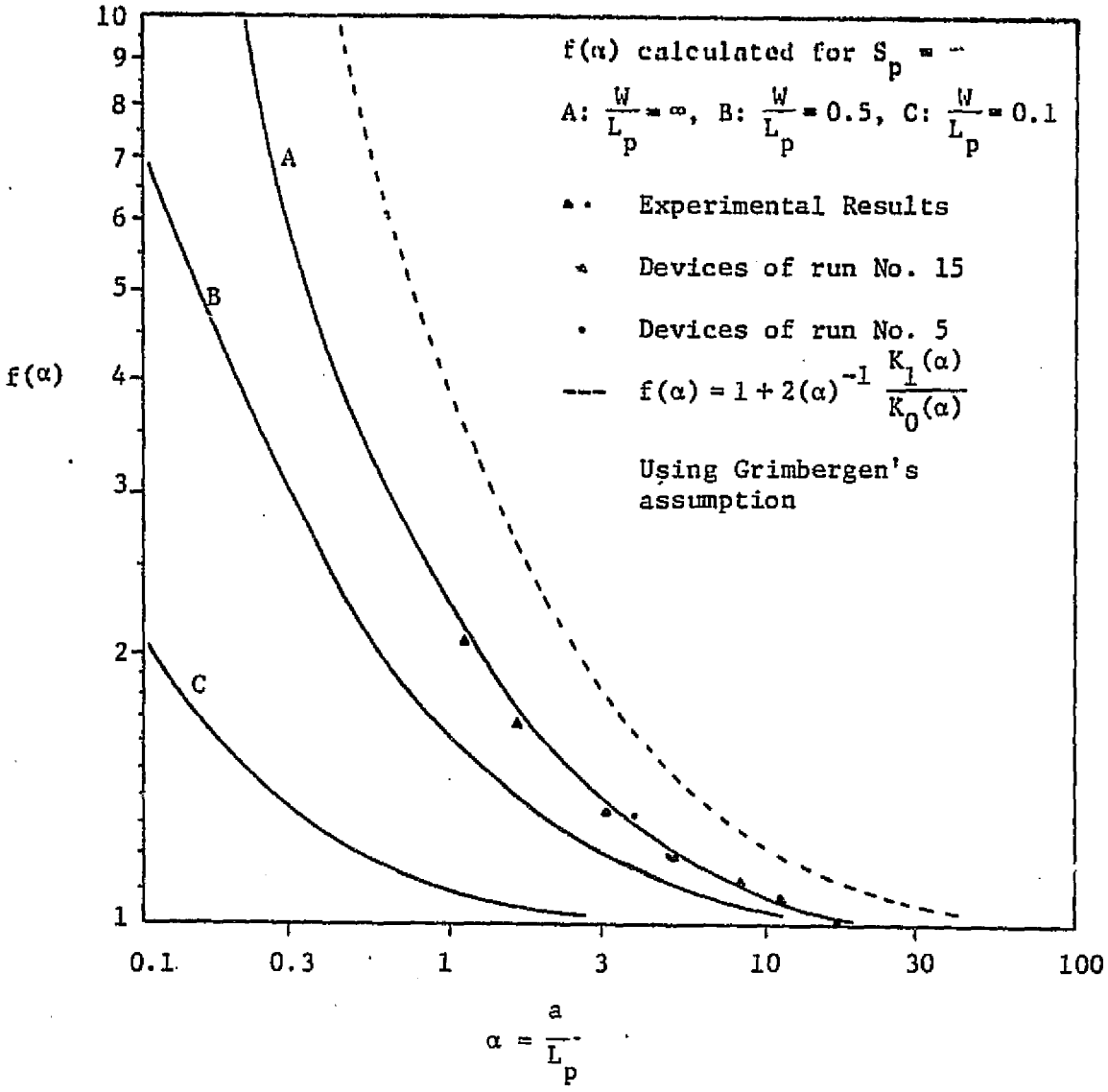

Figure 5.2.1 Normalized current density factor $f(\alpha) = J_\alpha/J_0$, as a function of the ratio of junction-area radius and diffusion length for $S_p = \infty$ at back contact.

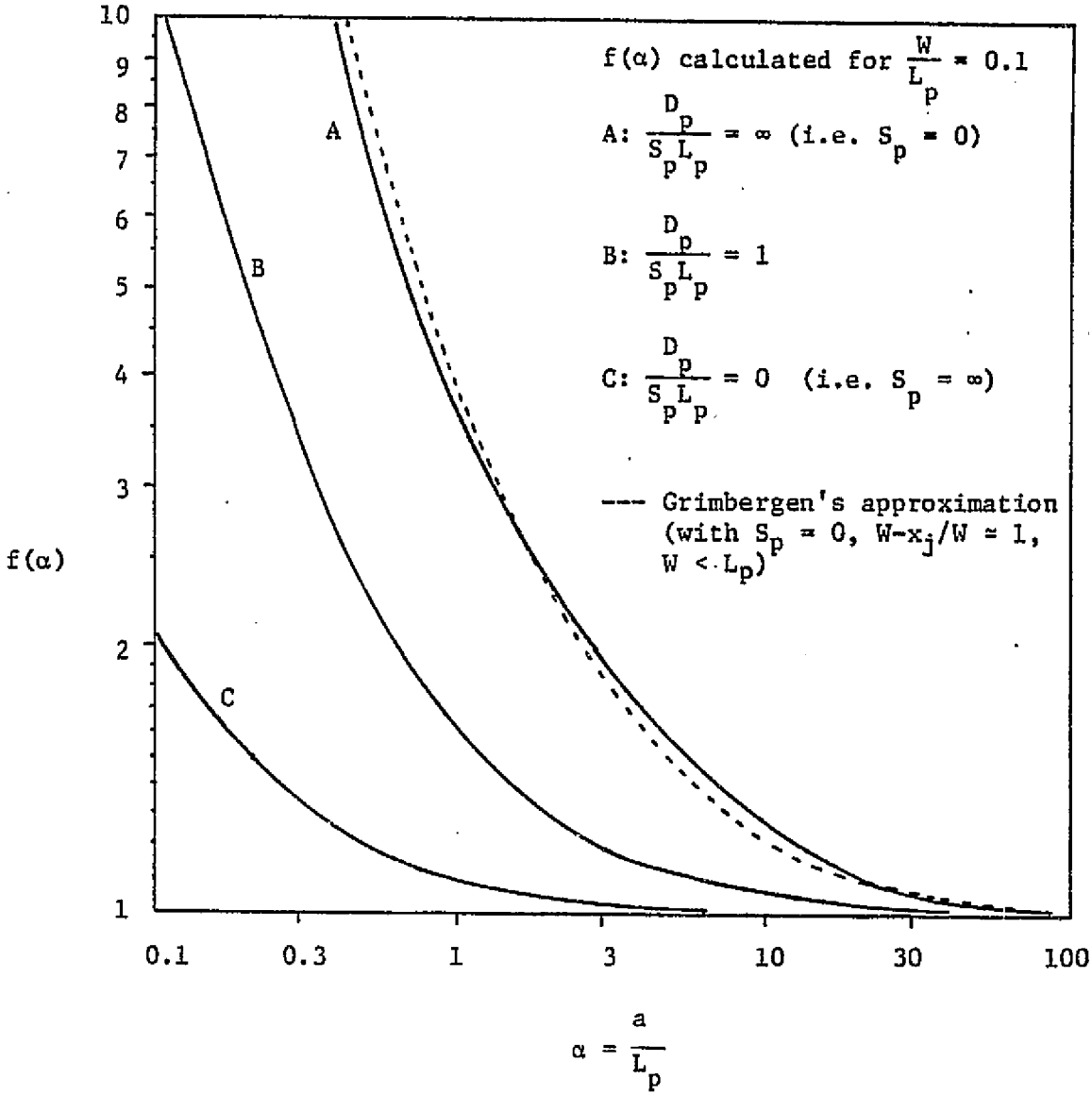

Figure 5.2.2 Illustrating that the detailed solution presented here (curve A) agrees well with Grimbergen's approximation for diodes for which $W/L_p \ll 1$, $S_p = 0$, and $(W - x_j)/W \simeq 1$.

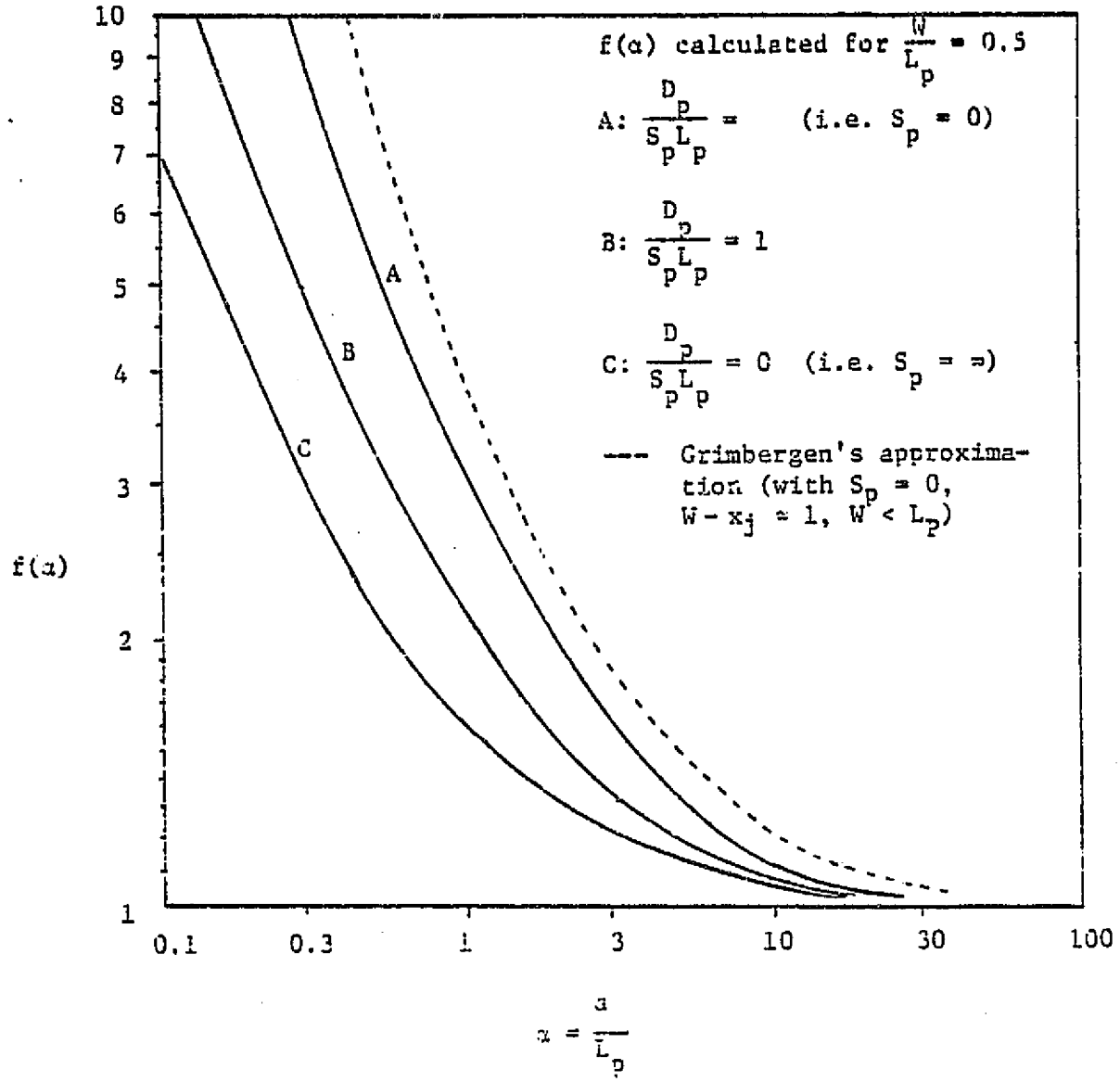

Figure 5.2.3 Illustrating that Grimbergen's approximation deviates from the detailed solution (curve A) for $W/L_p = 0.5$.

Table 5.1 Calculated $f(\alpha)$, $(f(\alpha) = J_\alpha/J_0)$, as a function of α, $\alpha = a/L_p$; β, $\beta = W/L_p$; and γ, $\gamma = D_p/S_pL_p$.

$f(\alpha)$		$\gamma = \frac{D_p}{S_pL_p}$ \ $\alpha = \frac{a_j}{L_p}$	0.1	0.3	1	3	10	30	100
	$\frac{W}{L_p} = 0.1$	∞		14.4	3.66	2.07	1.29	1.05	0.07
		5	27.04	6.92	2.31	1.37	1.11	1.03	
		1	10.24	3.37	1.59	1.18	1.06		
		0	2.15	1.32	1.08	1.03	1.0		
	$\frac{W}{L_p} = 0.5$	∞		9.19	3.05	1.59	1.12	0.97	
		1	13.48	4.89	2.02	1.31	1.08	1.01	
		0	7.03	2.9	1.58	1.23	1.06	1.0	
	$\frac{W}{L_p} >> 1$	0		5.8	2.2	1.36	1.08	1.03	0.98

5.3 Experimental Results

Using the experimental set-up of Fig. 5.3, we measured the current-voltage characteristic of p^+-n junction diodes with different areas, described in Table 5.2. For the measurement, the devices were heated inside a Statham furnace to a high enough temperature that the base recombination current dominates that from the junction space charge region, as evidenced by a unity slope on the (ln I) vs. (qV/kT) characteristics. The existence of a unity slope indicates that the current I is the sum of the recombination current from the quasi-neutral base and emitter regions. From the experiments [10] and reference [1], we know that the base recombination current dominates for our devices having a base doping concentration less than 10^{16} cm^{-3}.

Table 5.1 shows the current measurement on devices with seven different areas. Measurements are taken at a temperature of 375.5 ± 0.1°K and at a fixed forward bias of 0.3 volts. The base diffusion length of the devices obtained from X-ray measurement is L_{px} = 80 μm, and the substrate doping concentration is 1.25×10^{15} cm^{-3}.

Experimental results are compared with the theoretical predictions in Fig. 5.2. Good agreement is obtained.

5.4 Determination of Diffusion Length

As Chapter 3 has discussed, the diffusion length can be determined by (a) current measurement or (b) capacitance measurement. The methods of Chapter 3 hold directly provided $\frac{a}{L_p} >> 1$, i.e., they hold for the one-dimensional case only. If the device is small enough that $\frac{a}{L_p} >> 1$ is not true, then methods (a) and (b) must be altered as follows to include the dependence of P_n and J_p on two space dimensions.

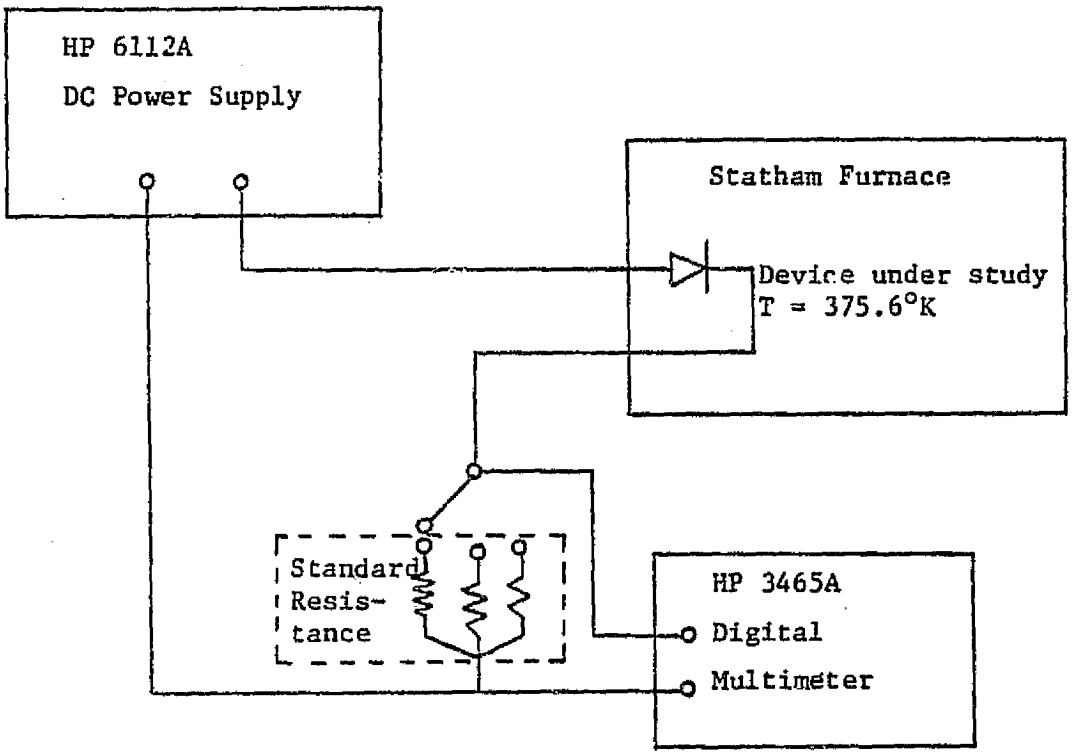

Figure 5.3 Block diagram for current measurement.

Table 5.2 Diffusion current I_α measured for seven devices having different values of $\alpha = a/L_{px}$. For these devices the one-dimensional current density is

$$J_0 = qD_p \frac{n_i^2}{N_{DD} L_{px}} \left(e^{\frac{qV}{kT}} - 1\right) = 5.91 \times 10^{-3} \text{ amp.}$$

The measured correction factor, J_α/J_0, shows excellent agreement with the correction factor, $f(\alpha)$, calculated from the solution to the two-dimensional boundary-value problem.

Diameters in Mills		100	70	50	30	20	10	7
I_α	(amp)	0.30×10^{-3}	0.16×10^{-3}	0.85×10^{-4}	0.32×10^{-4}	0.16×10^{-4}	0.47×10^{-4}	0.30×10^{-5}
$\alpha = \frac{a}{L_p}$		15.50	11.11	7.94	4.76	3.17	1.58	1.11
$J_\alpha = \frac{I_\alpha}{\pi a^2}$	(amp/cm^2)	5.92×10^{-3}	6.44×10^{-3}	6.7×10^{-3}	7.02×10^{-3}	7.89×10^{-3}	9.27×10^{-3}	1.21×10^{-3}
$\frac{J_\alpha}{J_0}$		1	1.09	1.13	1.19	1.34	1.57	2.04
$f(\alpha)$		1.03	1.06	1.11	1.22	1.36	1.75	2.15

Method (a): For devices for which the base recombination current greatly exceeds the emitter recombination current (for our devices if $N_B \leq 10^{16}$ cm^{-3}), the diffusion length can be determined by the following scheme. Suppose currents are measured (see Section 3) on devices 1 and 2 of radius a_1 and a_2, then

$$I_j = A_j J_{\alpha_j} = \pi a_j^2 J_{\alpha_j} = A_j \frac{J_{\alpha_j}}{J_0} J_0 = A_j J_0 \frac{J_{\alpha_j}}{J_0} = A_j J_0 f(\alpha_j) \quad (j = 1 \text{ or } 2) \tag{5.30}$$

where $\alpha_j = \frac{a_j}{L_p}$, and

$$J_0 = \frac{n_i^2}{N_{DD}} \frac{1}{L_p} \cdot e^{\frac{qV}{kT}} = \frac{C}{L_p} = g(L_p) \tag{5.31}$$

There are two equations and three unknowns. To find the value of L_p, an iterative procedure is used as follows. Try an initial value of L_p and calculate $\alpha_2 = \frac{a_2}{L_p}$, find the $f(\alpha_2)$ from the curve of Fig. 5.2. Plot $f(\alpha_1) = f(\alpha_2) \frac{J_{\alpha_1}}{J_{\alpha_2}}$. Notice whether $f(\alpha_1)$ is on the curve or not. If not, choose another L_p, check $f(\alpha_1)$ again. Continue this procedure until $f(\alpha_1)$ and $f(\alpha_2)$ both lie on the curve. The value of L_p producing this condition is the correct value of L_p. Note that good accuracy results provided α_1 and α_2 differ considerably. For example, $\alpha_2/\alpha_1 = 10$ and $\alpha_1 = 1$ yields accurate determination of L_p.

Method (b): If the emitter recombination current is comparable to that of the base (for $N_B \geq 10^{16}$ cm^{-3}), the above scheme is inappliacable. However, the capacitance method [1] still can be used to determine L_p. This method determines the base diffusion capacitance [11] which, for devices 1 and 2, is

$$C_{D_j} = \frac{dQ_{D_j}}{dV} = \frac{dQ_{D_j}}{dI_{D_j}} \cdot \frac{dI_{D_j}}{dv} = \frac{1}{\tau_j} \frac{dI_{D_j}}{dV} = \frac{1}{\tau_j} \frac{q}{kT} I_{D_j} \qquad (5.32)$$

$$(j = 1 \text{ or } 2)$$

But $\tau_1 = \tau_2$ for devices fabricated on the same wafer. Thus the determination of L_p from C_{D1} and C_{D2} is essentially the same as the determination from I_{D1} and I_{D2} described in (a) above. The theoretical curve of Fig. 5.2 therefore can also be used for the capacitance method of determining L_p.

In contrast to the methods of Section 5.4, which require two or more devices in determining the diffusion length, the diffusion length can be determined from measurements made on a single device by use of the following iterative procedure. First, L_p is estimated and the corresponding one-dimensional capacitance (or current) is calculated from (3.11) and multiplied by $f(\alpha)$ from Figures 5.2.1-5.2.3. The result is compared with the measured (two-dimensional) capacitance (or current). The procedure is continued until self consistency results.

5.5 Discussion

The diffusion length L_p as a function of temperature T can also be determined by use of Fig. 5.2. In contrast, the X-ray method does not readily yield L_p as a function of T because the small short circuit current (due to the small generation rate of X-ray) is obscured by the thermal noise signals existing in the device and contact wires. Thus the X-ray measurement of L_p is difficult at temperatures higher than room temperature.

Determination of the diffusion length by the current measurement is simple and accurate.

The validity of the theoretical calculation presented here can be checked by letting $\alpha \to 0$, and considering the special case in which the volume recombination vanishes. This produces the electric disk problem [5], illustrated in Fig. 5.1. For $\alpha = 0$, $a_0 = 1$, $a_2 = a_3 = a_4 = \ldots = 0$. Now let the earth ground plate be placed near the electric disk. For example, let $a/h = 20$, where a is the radius of the disk and h is the distance between disk and earth plate. Then, the average electric field calculated using section 5.2 is

$$E_{ave} = \frac{V}{h} \times 1.08 \tag{5.33}$$

where V is the potential of the disk. But, if $a/h \gg 1$, we know from electrostatics that $E \approx V/h$. Thus calculations using Section 5.2 are shown to agree with the results of the analogous electric disk problem.

In our theoretical calculation, we have approximated the shallow discussed junction by an infinitesimally thin disk. The current density becomes infinite at the edge of the junction, which is contrary to the condition occurring in actual diodes. The junction depth x_j shown in Fig. 5.4 is small but not equal to zero. As is shown in Appendix VI of Ref. [7], the current density at the junction edge can be expressed by

$$J_{EDGE} = qD_p \frac{P_n(x_j)}{L_p} \frac{K_0(\frac{x_j}{L_p})}{K_1(\frac{x_j}{L_p})} \tag{5.34}$$

where K_0 and K_1 are the modified Bessel functions of the third kind with orders zero and one, respectively.

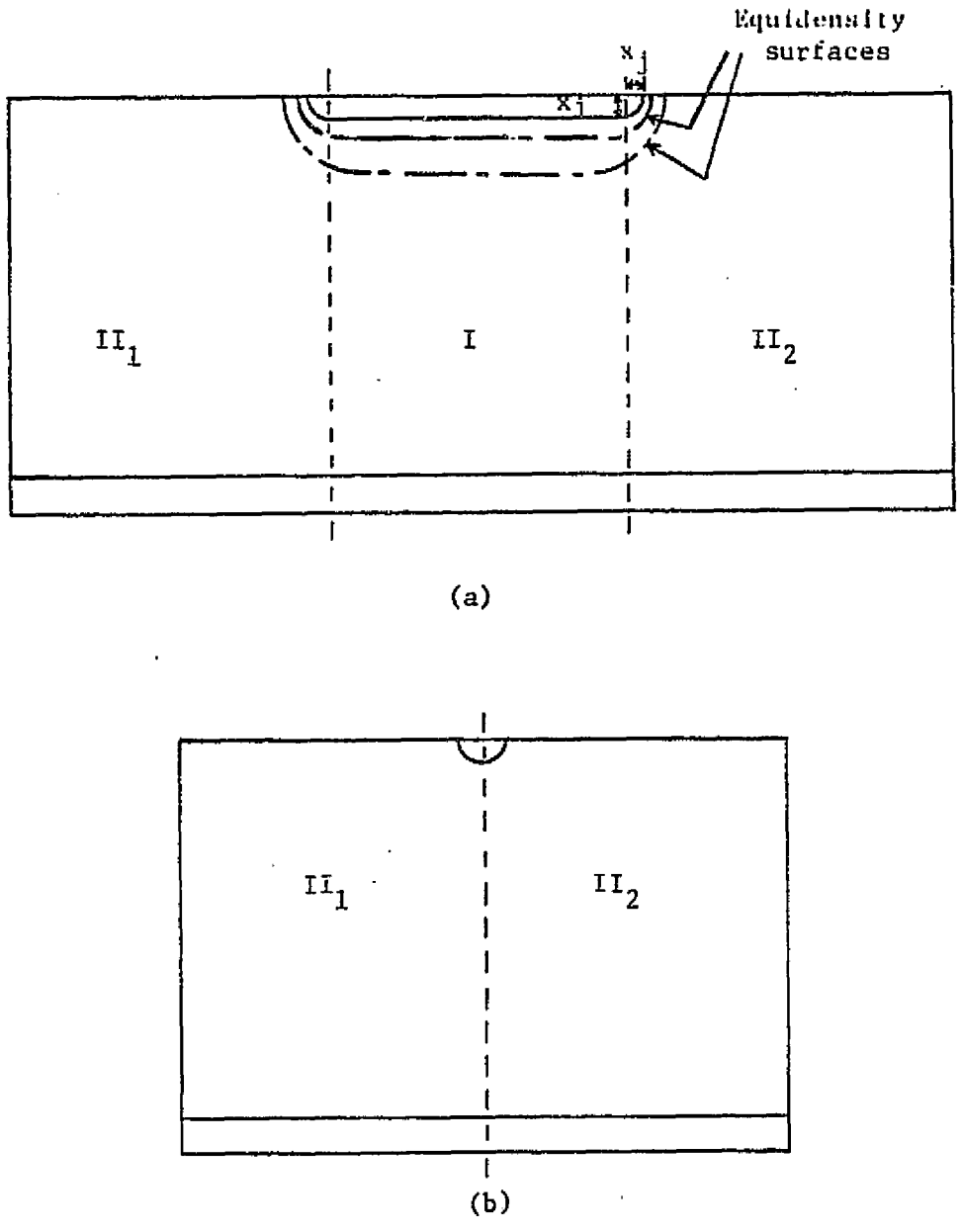

Figure 5.4 Exploitation of the symmetry in (a) leads to the simple boundary-value problem of (b), which yields an approximate solution for the edge (sidewall) current density.

REFERENCES FOR CHAPTER 5

1. A. Neugroschel, P.J. Chen, S.C. Pao, and F.A. Lindholm, "Diffusion length and lifetime determination in p-n junction solar cells and diodes by forward-biased capacitance measurements," IEEE Trans. Electron Devices, April 1978.

2. C.A. Grimbergen, "The influence of geometry on the interpretation of the current in epitaxial diodes," Solid State Electronics, Vol. 19, pp. 1033-1037, Dec. 1976.

3. J.H. Reynolds and A. Meulenberg, "Measurements of diffusion length in solar cells," J. Appl. Phys., Vol. 45, pp. 2582-2592, June 1974.

4. H.S. Carslaw and J.C. Jaeger, Conduction of Heat in Solids, Oxford University Press, London, 1959, pp. 214-216.

5. J.D. Jackson, Classical Electrodynamics, John Wiley & Sons, New York, 1972, pp. 90-93.

6. C.J. Tranter, Integral Transforms in Mathematical Physics, John Wiley & Sons, New York, 1959, pp. 111-123.

7. P.J. Chen, Ph.D. Thesis, Univ. of Florida (1978).

8. G.N. Watson, Treatise on the Theory of Bessel Functions, Cambridge, London, 1944.

9. M. Abramowitz and I.A. Stegun, Handbook of Mathematical Functions, Dover Publications, New York, 1970.

10. A. Neugroschel, F.A. Lindholm, and C.T. Sah, "A method for determining the emitter and base lifetimes in p-n junction diodes," IEEE Trans. Electron Devices, Vol. ED-24, pp. 662-671, June 1977.

11. W. Shockley, "The theory of p-n junctions in semiconductors and p-n junction transistors," Bell Syst. Tech. J., Vol. 28, pp. 435-489, July 1949.

PART III: INCREASING V_{OC} BY THE HLE STRUCTURE

CHAPTER 6 EMITTER CURRENT SUPPRESSION IN A HIGH-LOW-JUNCTION EMITTER SOLAR CELL USING AN OXIDE-CHARGE-INDUCED ELECTRON ACCUMULATION LAYER

INTRODUCTION: As Brandhorst first noted [1], the power conversion efficiency η seen in silicon p-n junction solar cells is considerably less than the maximum theoretical value of η mainly because the open-circuit voltage V_{OC} is smaller than simple p-n junction theory predicts. Experiments [2] on n^+-p silicon cells have shown that this discrepancy in V_{OC} results from the dominance, in the non-illuminated (dark) cell, of the emitter recombination current J_E over the base recombination current J_B. In cells having base doping concentrations of the order of 10^{17} cm^{-3}, for which the largest values of V_{OC} are seen, J_E exceeds J_B by about an order of magnitude [2], rather than being several orders of magnitude less than J_B as is predicted by simple p-n junction theory. The excess J_E has been attributed to the mechanisms [3] of energy band-gap narrowing and lifetime degradation that accompany heavy doping concentrations in the n^+ emitter.

To suppress J_E and thus raise the achievable value of V_{OC}, a new structure, the HLE junction solar cell, containing a high-low (H-L) junction in the emitter, has been proposed and its performance has been calculated on theoretical grounds [4,5]. The purpose of the present paper is to demonstrate, by experiment, that an H-L junction in the emitter created by an oxide-charge-induced electron accumulation layer can completely suppress J_E. We call this device the oxide-charge-induced, high-low-junction emitter (OCI-HLE) solar cell. For the particular structure studied, under AM1 or AM0 illumination, this suppression increases V_{OC} considerably over the values seen in a conventional n^+-p solar cell of the same base doping concentration. Larger increases in V_{OC} are to be expected. These expectations are discussed together with the advantages inherent in this type of HLE solar cell.

THE STRUCTURE: As is shown in Fig. 1, the H-L junction in the emitter results from an electron accumulation layer induced in the n-type epitaxial emitter region by a positive oxide charge Q_O. The charge Q_O is created near the $Si-SiO_2$ interface during a low temperature oxygen heat treatment [6-8]. To assure a good ohmic contact, a shallow n^+ diffusion is made under the metallized portion of the top surface area. This n^+ diffusion also provides a high-low-barrier and a small effective surface recombination velocity [9] for holes. The p-type base has a doping concentration $N_{AA} \simeq 5x10^{17}$ cm^{-3}, which approximately minimizes J_B in a cell without a back-surface field [10]. For good cell performance, the n-type epitaxial region must satisfy four conditions: (a) it must be thick enough and doped heavily enough to provide the sheet conductance needed to make the series resistance negligible; (b) its doping concentration must be low enough (less than about 10^{17} cm^{-3}) to avoid the effects of energy band gap narrowing and severe hole lifetime degradation; (c) its hole lifetime must be long enough that nearly all the holes injected from the base diffuse through to the surface rather than recombining within the region; and (d) the surface recombination velocity under the oxide should be low.

The mechanisms underlying the suppression of J_E are simple. As the injected holes diffuse into the electron accumulation layer, the partially reflecting boundary condition [9] at the H-L junction depresses the hole density so that the hole recombination current is controlled by the electron concentration N_S near the surface and the hole surface recombination velocity S_p:

$$J_E \simeq (qn_i^2 S_p/N_S)[\exp(qV/kT) - 1] \qquad (1)$$

Here S_p is the surface recombination velocity at the Si-SiO_2 interface covering the non-metallized portion of the device surface area; S_p can be orders of magnitude less than the surface recombination velocity at an Ohmic contact. As (1) suggests, if the ratio S_p/N_S is small enough, J_E will be suppressed well below J_B.

The oxide-charge-induced H-L structure of Fig. 1 is an attractive realization of the HLE solar cell because it avoids high concentrations of donor impurity atoms in the thin H layer near the surface. This eliminates heavy-doping effects [3] such as band-gap narrowing and hole lifetime degradation in the H layer and it may help the achievement of low values of S_p. The avoidance of a diffusion step to form a highly-doped H layer eliminates, over the non-metallized portion of the surface area, the diffusion of unwanted impurities and vacancies into the silicon along with the donor atoms. From the viewpoint of cell performance, these properties suggest that the OCI-HLE solar cell can exhibit good blue response in addition to increased V_{OC}.

CELL FABRICATION: Several runs of test cells were made that demonstrate the desired J_E suppression. In one such run, the starting material consisted of a 10μm thick n-type layer of resistivity $\rho_{epi} \simeq 0.1$ Ωcm grown epitaxially on a p-type substrate of 300μm thickness and resistivity $\rho_{base} \simeq 0.1$ Ωcm.

The wafer was oxidized in dry O_2 with 0.3% TCE at 1100°C to grow a 2500Å thick oxide layer, which was later etched to 1100Å to improve the anti-reflection properties. The temperature of 1100°C was chosen for this test cell to assure a good-quality oxide and a low value of S_p. After oxidation the wafer was cooled from 1100°C to 1000°C at the rate of 30°C per hour and then cooled to 700°C in three hours. Holes were opened in the oxide for an n^+

contact diffusion done at 900°C for 20 minutes. The device was then heated in dry oxygen for 2 hours at 700°C to increase the oxide charge density Q_o [6-8].

A second run employed similar processing but used starting material with $\rho_{epi} \simeq 1.4$ Ωcm and $\rho_{base} \simeq 0.14$ Ωcm.

EXPERIMENTAL DEMONSTRATION OF J_E SUPPRESSION AND LARGE V_{OC}: Since the oxide charge Q_o is near the Si-SiO_2 interface, the total charge accumulated in the silicon is $Q_s \simeq Q_o$. The electron distribution is described by MOS theory [11]. The electron surface concentration is about 3×10^{18} cm^{-3} ($\rho_{epi} \simeq 0.1$ cm) and about 2×10^{18} cm^{-3} ($\rho_{epi} \simeq 1.4$ cm). Most of the electrons in the accumulation layer reside within about three Debye lengths (about 100Å) from the surface.

The base diffusion length L_n, measured by X-ray excitation [12], was $L_n \simeq 20\mu m$ for devices from the first run and $L_n \simeq 30\mu m$ for devices from the second run. Measurement of the dark I-V characteristics showed for both runs that the ideal saturation current (determined by subtracting the space-charge-region recombination current [2]) was equal, within measurement error, to the base recombination current J_B calculated from knowledge of L_n. This demonstrates that $J_E << J_B$. Thus V_{OC} is determined mainly by J_B in these devices. The results of the measurements show further that the emitter saturation current J_{EO} is suppressed to less than about 5×10^{-14} A/cm^2, which corresponds to a voltage, $(kT/q)\ln(J_{SC}/J_{EO}) \geq 705$ mV, for $J_{SC} = 35$ mA/cm^2 (measured in these devices). Thus J_E is suppressed to values so low that it presents no barrier to the achievement of $V_{OC} \simeq 700$ mV, which is the maximum value of V_{OC} predicted by classical theory for a 0.1 Ωcm base resistivity for AMO illumination.

The performance of the test cells was measured at NASA Lewis Research Center. The cell of the first run showed the largest V_{OC}: V_{OC} = 634 mV at 25°C. Because this test cell had much larger metal coverage on the illuminated surface (total area = A_T = 1.34 cm^2; non-metallized area = A_N = 0.972 cm^2) than the 5% metallized area of a cell optimized for AMO illumination, the measured V_{OC} should be corrected to account for the loading effect of the parasitic p-n junction diode under the metallized portion of the surface. The correction, estimated from $\Delta V_{OC} = (kT/q)[\ell n(A_T/A_N)]$, is about 8 mV. Thus this OCI-HLE cell has an open circuit voltage of 642 mV at 25°C for AMO illumination. This compares with the largest values of V_{OC} = 610 mV previously reported for n-on-p silicon p-n junction solar cells [2,13].

PROJECTIONS: As was emphasized, because J_E is completely suppressed, V_{OC} of these OCI-HLE solar cells depends mainly on J_B, which is approximately inversely proportional to L_n. Cells of about 0.1 Ωcm base resistivity have shown L_n of approximately 100 μm [2,14] which is much larger than the values of L_n measured for our OCI-HLE test cells. These low values of L_n may result from several origins. First, in the test cells, we grew SiO_2 at 1100°C to assure low values of S_p and complete suppression of J_E at the possible expense of L_n. Second, the starting epitaxial material had poor values of L_n. For example, the value of L_n measured on the epitaxial p-n junction prior to oxidation and other processing steps was only about 30 μm for the material used to fabricate the test cells of the first run. We are trying to increase L_n and thus V_{OC} by several approaches, including the growth of SiO_2 at lower temperatures, the use of better quality starting material, and the use of a back-surface-field [10] in conjunction with

higher values of base resistivity. An additional improvement in V_{OC} can be expected from improvements in the short-circuit current density J_{SC}, which will be discussed below. When all of the potential improvements are combined, the projected maximum value of V_{OC} is about 700 mV at about 25°C.

The measured value of the fill factor FF at 25°C was 0.802. The value of FF increases as V_{OC} increases, and the projected maximum FF, corresponding to V_{OC} = 700 mV, is about 0.83 [15].

The best measured value of J_{SC} of these test cells was 35 mA/cm^2. This value resulted even though no special attention was given to achieving good anti-reflection (AR) properties and even though the small L_n implies poor collection from the longer wavelengths of the solar spectrum. Good blue response was measured at a wavelength of 0.5 μm. Improvements in J_{SC} will result from improvements in L_n and the AR properties. The maximum J_{SC} is expected to occur in OCI-HLE cells made with higher base resistivity (about 10Ωcm) and a back-surface field, as in the Helios cell for which J_{SC} = 40 mA/cm^2 [16]. The projected maximum J_{SC} is about 40 mA/cm^2.

These projections correspond to an AM0 maximum power conversion efficiency of OCI-HLE solar cells in the 17 to 18 per cent range, which contrasts with the maximum efficiency now seen in the silicon p-n junction solar cells of about 15% [16]. Because of spectral differences, the AM1 efficiency is higher than the AM0 efficiency. The projected maximum efficiency of the OCI-HLE solar cell for AM1 illumination is about 20%. High efficiencies also can be expected in OCI-HLE solar cells designed for concentrated sunlight illumination in the range of 25 to 100 suns [17].

REFERENCES

1. H.W. Brandhorst, Jr., Record of 9th Photovoltaic Specialists Conf., 1, (1972).
2. F.A. Lindholm, A. Neugroschel, C.T. Sah, M.P. Godlewski, and H.W. Brandhorst, Jr., IEEE Trans. Electron Devices, ED-24, 402 (1977).
3. F.A. Lindholm and C.T. Sah, IEEE Trans. Electron Devices, ED-24, 299 (1977); C.T. Sah and F.A. Lindholm, IEEE Trans. Electron Devices, ED-24, 358 (1977).
4. C.T. Sah, F.A. Lindholm, and J.G. Fossum, IEEE Trans. Electron Devices, ED-25, 66 (1978).
5. J.G. Fossum, F.A. Lindholm, and C.T. Sah, Tech. Digest 1977 Int. Electron Devices Mtg., 225 (1977).
6. B.E. Deal, M. Sklar, A.S. Grove, and E.H. Snow, J. Electrochem. Soc., 114, 266 (1967).
7. H.S. Fu and C.T. Sah, IEEE Trans. Electron Devices, ED-19, 273 (1972).
8. C.T. Sah, T.N. Ning, and L.L. Tschopp, Surface Science, 32, 561 (1972).
9. J.R. Hauser and P.M. Dunbar, Solid-State Electron., 18, 715 (1975).
10. J. Mandelkorn and J.H. Lamneck, Jr., Record of 9th Photovoltaic Specialists Conf., (1972).
11. R.H. Kingston and S.F. Neustadler, J. Appl. Phys., 26, 718 (1955).
12. W. Rosenzweig, Bell Syst. Tech. J., 41, 1573 (1962).
13. M.P. Godlewski, H.W. Brandhorst, Jr., and C.R. Baraona, Record of 11th IEEE Photovoltaic Specialists Conf., 32 (1975).
14. S.C. Pao, unpublished.
15. M.A. Green, Solid-State Electron., 20, 265 (1977).
16. H.W. Brandhorst, Jr., 1975, Int. Electron Device Mtg., 111 (1975).
17. F.A. Lindholm, J.G. Fossum, A. Neugroschel, S.C. Pao, and C.T. Sah, 13th IEEE Photovoltaic Specialists Conf., Session XV, June 8, 1978.

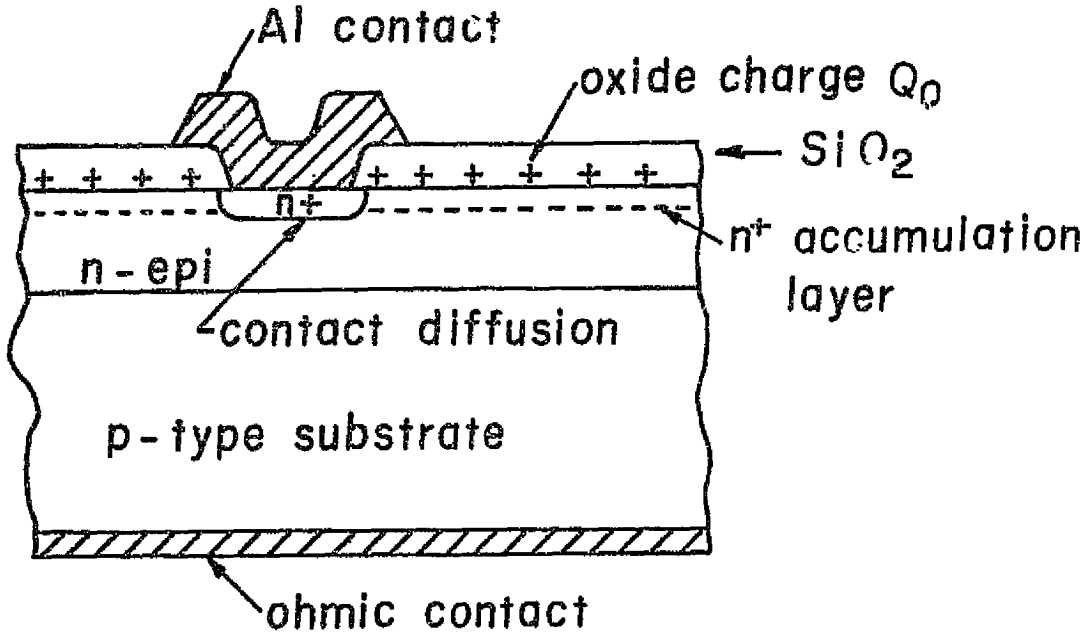

Fig. 1 Cross section of an oxide-charge-induced high-low emitter (OCI-HLE) solar cell. Electron accumulation layer is induced by a positive oxide charge Q_o.

CHAPTER 7 DISCUSSION

This report contains the results of research in transition. The first two parts of the report deal with theory and experiment aimed toward an investigation of the basic mechanisms responsible for low V_{OC} in n-on-p solar cells. The third part describes a new device structure that suppresses the emitter current and raises V_{OC} well above values seen before. Our NASA LeRC research now is fully focussed on the work described in the third part. In subsequent reports, we will describe in more detail the theory underlying the operation of HLE devices, both OCI and diffused, and will give the results supplied by our ongoing experiments in HLE solar cells.